

**Determination of Optical Path Lengths  
in Scattering Media by Intensity Modulated Light  
in Connection with  
Gas in Scattering Media Absorption Spectroscopy**

Master's thesis  
by  
Henrik Fält

Lund Reports on Atomic Physics, LRAP-323  
Department of Physics, Lund Institute of Technology  
Lund, June 2004

## Abstract

A frequency resolved method for determination of optical path lengths in scattering media has been implemented. In the method, scattering-induced phase shifts in amplitude modulated light are measured. The phase shifts are combined with a diffusion model for light transport in order to determine the optical path lengths. A system for gas in scattering media absorption spectroscopy has been realized, suitable for oxygen.

# Contents

<b>1. Introduction . . . . .</b>	<b>7</b>
<b>2. Diode Lasers . . . . .</b>	<b>9</b>
2.1 Diode Laser Characteristics . . . . .	9
2.1.1 Principle of Operation. . . . .	10
2.1.2 Optical Properties . . . . .	12
<b>3. Phase Measurement Systems . . . . .</b>	<b>13</b>
3.1 Signal Theory . . . . .	13
3.1.1 Filters . . . . .	15
3.1.2 Power Splitters . . . . .	16
3.1.3 Mixers. . . . .	16
3.2 Theory of Modulation Systems . . . . .	17
3.2.1 Homodyne Modulation Systems . . . . .	17
3.2.2 Heterodyne Modulation Systems. . . . .	19
3.2.3 Single Side Band Modulation Systems. . . . .	22
<b>4. Light Propagation in Scattering Media . . . . .</b>	<b>27</b>
4.1 Fundamental Interactions of Light and Matter . . . . .	27
4.1.1 Reflection . . . . .	27
4.1.2 Absorption . . . . .	28
4.1.3 Scattering . . . . .	28
4.2 Light Transport Theory . . . . .	29
4.2.1 Time and Frequency Domain Solutions . . . . .	29
4.2.2 Diffusion Model for Light Transport. . . . .	31
<b>5. Gas in Scattering Media Absorption Spectroscopy (GASMAS) . . .</b>	<b>33</b>
5.1 Absorption Spectroscopy . . . . .	33
5.1.2 Wavelength Modulation. . . . .	33
5.2 The GASMAS Method. . . . .	34
5.2.1 The GASMAS Setup. . . . .	34
5.2.2 GASMAS Measurements . . . . .	36

<b>6. Diagnostics of Laser Diodes . . . . .</b>	<b>39</b>
6.1 Diagnostical Setup and Method. . . . .	39
6.1.1 SHARP Laser Diode LT031MDO 0-30 . . . . .	39
6.1.2 Roithner Lasertechnik Laser Diodes. . . . .	41
6.2 Diagnostic Results . . . . .	42
6.2.1 SHARP Laser Diode LT031MDO 0-30 . . . . .	42
6.2.2 Roithner Lasertechnik Laser Diodes. . . . .	44
<b>7. Setup of a GASMAS System . . . . .</b>	<b>45</b>
7.1 Fibre Coupling . . . . .	45
7.2 The Setup . . . . .	47
7.3 Measurements on Wheat Flour . . . . .	49
<b>8. Phase Measurements on Polystyrene Foam . . . . .</b>	<b>51</b>
8.1 Setup of a Homodyne Measuring system . . . . .	51
8.2 Method of Phase Measurements . . . . .	53
8.2.1 Measurement Procedure . . . . .	53
8.2.2 Data Evaluation . . . . .	53
8.3 Preliminary Measurements . . . . .	54
8.3.1 Basic Results . . . . .	54
8.3.2 Evaluation. . . . .	57
8.4 Extensive Measurements . . . . .	57
8.4.1 Basic Results . . . . .	58
8.4.2 Evaluation. . . . .	60
8.5 Optical Properties of Polystyrene Foam . . . . .	61
<b>9. Summary and Conclusions . . . . .</b>	<b>65</b>
9.1 Experimental Results. . . . .	65
9.1.1 Laser Diodes . . . . .	65
9.1.2 GASMAS Setup . . . . .	65
9.1.3 Phase Measurements on Polystyrene Foam . . . . .	65
9.2 Future Work. . . . .	66
<b>Acknowledgements . . . . .</b>	<b>67</b>
<b>References . . . . .</b>	<b>69</b>
<b>Appendix A . . . . .</b>	<b>71</b>



# 1. Introduction

As soon as the lasers were introduced in the 1960's, they found their way into the field of spectroscopy. The development of tuneable lasers was particularly important. An atom or molecule of choice could be studied just by tuning the laser to the right wavelength. Such studies have been done for various applications; from pure atomic or molecular physics, to detection of atmospheric pollutants or diagnosis of cancer.

Apart from being used in CD players and bar-code readers, diode lasers can be used to highly reduce the size and cost of spectroscopic experiments. Diode lasers are also beneficial with their simple operation, wavelength tuning and ability to be modulated up to high frequencies.

Absorption spectroscopy is a powerful tool to monitor free gases. This has before been restricted to cases where the gas has been the sole component of the sample or when it has been inside a material almost free from scattering. In 2001, a technique was presented that made it possible to measure the free gas content embedded in scattering materials. The technique is called Gas in Scattering Media Absorption Spectroscopy, or GASMAS for short. The materials can be of either organic or synthetic nature. Measurements have been done on such materials as wood, apples, marble, polystyrene foam, etc. Although the total amount of absorption is fairly easy to measure, one has to investigate how far the light has travelled through the material in order to determine the concentration of gas inside the sample. In a non scattering medium this is easy; it is just to measure the thickness of the sample, but in other media the path of the light can get significantly longer because of the scattering. The presence of scattering, characterized by a scattering coefficient,  $\mu_s$ , complicates the measurement of absorption, characterized by an absorption coefficient,  $\mu_a$ . However, it is possible to 'orthogonalize' the absorption and scattering phenomena by suitable experimental techniques. There are mainly three methods available; time resolved, spatially resolved, and frequency resolved spectroscopy.

The primary aim of the project, accounted for in this thesis, was to implement a frequency resolved method. The method should, by measuring the phase shifts in amplitude modulated light and applying a model of light transport in scattering media, determine the optical path lengths in scattering media. It should also be done in such a way so that it was able to be a part of a GASMAS setup. A request was also that a new GASMAS system for molecular oxygen measurements was to be set up using some newly purchased equipment. In connection to that, a suitable laser diode had to be found.

This thesis contains four theoretical and three experimental chapters. In the first theoretical chapter, the principles of lasers diodes are being presented. The second one treats signal theory and some modulation systems that can be used for phase measurements. The possibility to calculate path lengths from phase shifts is treated next. The theoretical part is concluded with a description of the GASMAS technique. The experimental part begins with diagnostics of a number of laser diodes to see whether they could be used for absorption spectroscopy of molecular oxygen or not. Then the setup of the new GASMAS system is described, as well as an attempt to measure the concentration dependence of GASMAS signals in wheat flour. Finally, phase measurements on polystyrene foam with the intent to determine the optical path length, are presented.

The work that is presented in this master's thesis has been carried out in the molecular spectroscopy group at the Atomic Physics Division of the Lund Institute of Technology.

## 2. Diode Lasers

The first laser that was made operable was a ruby laser. The year was 1960. Only two years after, the first diode lasers, or semiconductor lasers, were demonstrated. The first diode lasers had to be operated in cryogenic temperatures,  $< 100$  K. Since the development boom in the 1980's many diode lasers can now be run at room temperature. It was the applications in the fields of, e.g., optical communications and data storage, that lead to this boom. The commercial demands are still what dictates the availability of what types of lasers one can get on the market.

### 2.1 Diode Laser Characteristics

Compared to other types of lasers, diode lasers have many advantages apart from their compact size. They have a high efficiency (about 20% or more), a long life time, easy operation, high reliability, and they are relatively cheap. Abilities that are used in spectroscopy are that they have a high spectral purity and wavelength stability. Diode lasers can also be easily tuned in wavelength as well as modulated at high frequencies, commonly up to 1 GHz [1].

Diode lasers can be found from about 400 nm up to 30  $\mu\text{m}$ . In the visible and near-infrared (NIR) range (0.4-2.0  $\mu\text{m}$ ), the spectral region of interest for this thesis, the diode lasers consist of semiconductor materials from group III (Al, Ga, In) and V (N, P, As, Sb) of the periodic table. However, the spectral regions covered, are quite incomplete. [2]

### 2.1.1 Principle of Operation

Diode lasers are made in a variety of styles. A common type of laser is shown in Fig. 2.1. It is index guided with a double heterostructure. The active medium, i.e. where the laser light is produced, is placed between two other semiconductor materials with higher band gap energies. When applying a current to the p-n junction, electrons and holes are created in the active layer. When these recombine, light is produced. If the current is above a threshold value, a population inversion is achieved and the structure can begin to work as a laser. When the current is lower than the threshold, the diode will still emit light, but since the losses are too high to achieve a population inversion it will emit light as an ordinary light emitting diode.

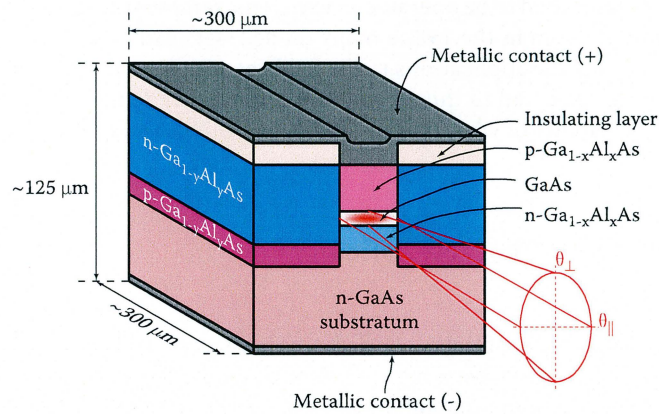


Figure 2.1: Illustration of a typical double-heterostructure index guided diode laser. Typical sizes and layer materials are shown, as well as the divergence and asymmetry of the laser beam. (From information from Ref. [2].)

When the temperature is increased the losses will also increase and the threshold current will thus be higher. This can be seen in Fig. 2.2. The temperature is often controlled with a Peltier element. Although the diodes can be operated between 0 °C and 60 °C or above, one usually keeps the temperature between 10 °C and 50 °C, to avoid water condensation, and thermal degradation [3]. The threshold current at a certain temperature is proportional to the exponential of the ratio between this temperature and a nominal temperature, which is specific to the laser diode being used [2].

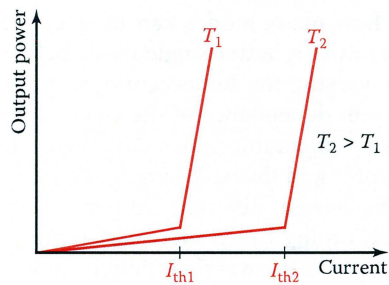


Figure 2.2: Illustration of output power versus current from a diode laser operated at two different temperatures. The diode is starting to lase at the two threshold currents  $I_{th1}$  and  $I_{th2}$ , respectively.

In order to get the laser feedback, reflective front and back surfaces are made, usually by splitting the diode along its crystal planes. The surfaces reflect because of the different refractive indices of the air and the semiconductor material. Sometimes these surfaces are clad with reflective coatings to get higher output powers. Behind the diode, a monitoring photo diode is placed, that gives a monitoring current proportional to the laser output power.

In the vertical direction the transverse modes, roughly the spatial distribution of the light, are restricted by a change in the refractive index due to the different materials. In the horizontal direction there are two ways of restricting these modes. In the first, gain guiding, the wave guide is determined by changes in the refractive index due to changes in the carrier concentration. However, a better technique is the index guiding, where the variations in the refractive index is accomplished by changes in the material structure.

### 2.1.2 Optical Properties

When a beam of light exits a laser diode it has quite imperfect properties. It is divergent, asymmetric and astigmatic. The astigmatism, though, is rather small for modern index guided lasers in the visible or NIR region. The divergence and asymmetry originates from the shape of the active region; the divergence from the small size and the asymmetry from the rectangular shape. The divergence is typically  $10\text{-}20^\circ$  in the horizontal plane and  $30\text{-}40^\circ$  in the vertical plane [3]. These effects can be corrected with an appropriate lens system.

The cavity length is much larger than the wavelength of the light, which makes it possible for many longitudinal modes to exist. It is the material gain profile that determines how many modes can exist at the same time. Usually index guided diode lasers exhibit better single mode behaviour. The wavelength can be altered either by varying the temperature of the semiconductor or the driving current. The current dependence of the wavelength is really an effect of the change in the junction temperature caused by the current. The temperature changes both the gain profile and the path length, the latter because of a change in the refractive index. Because of different temperature dependencies of these phenomena a wavelength tuning by an increased temperature will result in a partially continuous increase of the wavelength with sudden jumps between the longitudinal modes. Such a tuning can be seen in Fig. 2.3. For an AlGaAs diode laser, a typical change in the gain profile is about  $0.25\text{ nm}/^\circ\text{C}$  while the optical length changes with about  $0.06\text{ nm}/^\circ\text{C}$  [3]. It is preferable to coarsely tune the lasers wavelength with the temperature, and to fine tune with the current.

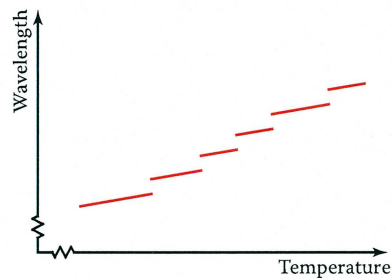


Figure 2.3: Schematic illustration of the change of wavelength, for a laser diode, as the temperature is changed. The sudden steps in the wavelength are the mode jumps.

### 3. Phase Measurement Systems

In order to retrieve phase information from a modulated source with a high accuracy it is necessary to use a good detection system. There are some different techniques available, mainly coming from communication technologies. In this text three basic techniques are described; homodyne, heterodyne and single side band (SSB) modulation systems. To begin with, some signal theories concerning the different components of these systems are explained.

#### 3.1 Signal Theory

If  $w(t)$  is a signal in time domain then

$$W(\omega) = \mathcal{F}w(t) = \int_{-\infty}^{\infty} w(t)e^{-i\omega t} dt \quad (3.1)$$

is defined as its Fourier transform. The inverse Fourier transform is defined as

$$w(t) = \mathcal{F}^{-1}W(\omega) = \frac{1}{2\pi} \int_{-\infty}^{\infty} W(\omega)e^{i\omega t} d\omega. \quad (3.2)$$

To calculate the absorption and scattering coefficients we need the phase shifts of sinusoidal signals. Therefore it is preferable to work with signals that look like

$$x(t) = A + B\cos(\omega_0 t + \phi). \quad (3.3)$$

Here  $\omega_0$  is the angular frequency and  $\phi$  is the phase.  $A$  and  $B$  are real constants. Then

$$X(\omega) = 2\pi A\delta(\omega) + \pi B\left(e^{i\phi}\delta(\omega - \omega_0) + e^{-i\phi}\delta(\omega + \omega_0)\right) \quad (3.4)$$

will be the representation of the signal in frequency domain. Figure 3.1 and 3.2 show the signal,  $x$ , in the time and frequency domain, respectively.



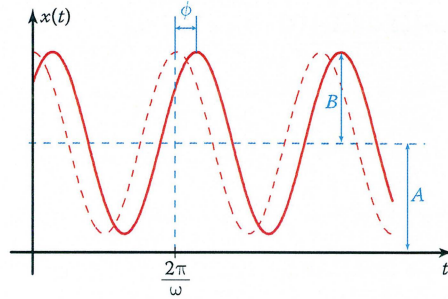


Figure 3.1: The signal  $x(t)$  in the time domain as defined in the text.

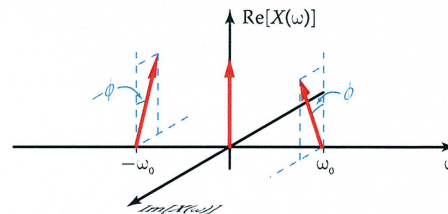


Figure 3.2: The signal  $X(\omega)$  in frequency domain as defined in the text.

The impulse response,  $h(t)$ , for a linear time invariant system  $\mathcal{S}$  is the system response to a Dirac delta function,  $\delta(t)$ .

$$\delta(t) \rightarrow \boxed{\mathcal{S}} \rightarrow h(t) = \mathcal{S}[\delta(t)] \quad (3.5)$$

If a signal  $w(t)$  is sent into a system  $\mathcal{S}$  with impulse response  $h(t)$  then the output signal  $y(t)$  is

$$w(t) \rightarrow \boxed{\mathcal{S}} \rightarrow y(t) = \mathcal{S}[w(t)] = h(t) * w(t) \quad (3.6)$$

where  $*$  is the convolution sign. From the frequency point of view it will look like

$$W(\omega) \rightarrow \boxed{\mathcal{S}} \rightarrow Y(\omega) = \mathcal{S}[W(\omega)] = H(\omega)W(\omega) \quad (3.7)$$



### 3.1.1 Filters

The most basic types of filters are low-, high- and band pass filters. Described in terms of frequency components, a filter is a system that rejects some frequencies while letting others pass.

An ideal low pass filter (LPF) passes frequencies up to some cut off frequency,  $\omega_c$ .

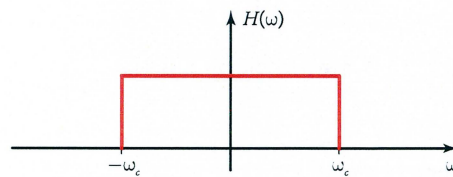


Figure 3.3: An ideal low pass filter.

An ideal high pass filter (HPF) is the opposite. It passes frequencies above a cut off frequency,  $\omega_c$ .

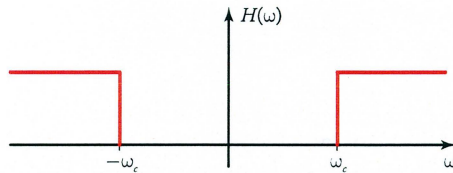


Figure 3.4: An ideal high pass filter.

The third type of filter, band pass filters (BPF), passes frequencies between two cut-off frequencies,  $\omega_{c1}$  and  $\omega_{c2}$ .

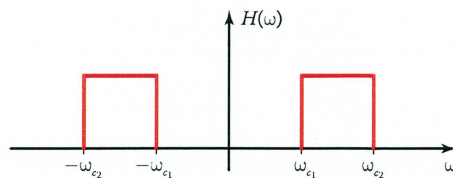


Figure 3.5: An ideal band pass filter.

In reality the transition between pass band and stop band is not that sharp. A better model of a filter would be one according to Fig. 3.6.

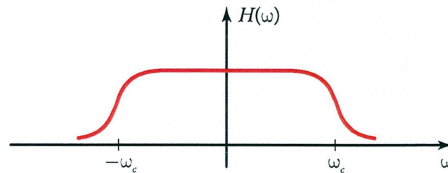


Figure 3.6: A more realistic low pass filter.

### 3.1.2 Power Splitters

The mean power of a signal  $w(t)$  is defined as

$$P(w(t)) = \lim_{\tau \rightarrow \infty} \frac{1}{2\tau} \int_{-\tau}^{\tau} |w(t)|^2 dt \quad (3.8)$$

which for a periodic signal is equal to

$$P(w(t)) = \frac{1}{T} \int_T |w(t)|^2 dt \quad (3.9)$$

where  $T$  is the period time for the signal. A lossless, equally dividing power splitter splits a signal into two equal signals with half of the power compared to the input signal. For the sinusoidal signal  $x(t)$  defined above, the power splitting system works according to

$$\begin{array}{c}
 x(t) = A + B\sin(\omega_0 t + \phi) \longrightarrow \boxed{\mathcal{S}} \begin{array}{l} \xrightarrow{y_1(t) = \mathcal{S}[x(t)] = \frac{1}{\sqrt{2}}x(t)} \\ \xrightarrow{y_2(t) = y_1(t)} \end{array}
 \end{array} \quad (3.10)$$

### 3.1.3 Mixers

A mixer is a nonlinear system which creates the sum and the difference frequencies of the input signals. Mathematically, this system is equivalent to a multiplication of the signals. The following shows a mixing between two signals  $x_1(t)$  and  $x_2(t)$ . For simplicity they are defined as purely sinusoidal without zero frequency components.

$$\begin{array}{l}
 x_1(t) = A_1 \cos(\omega_1 t + \phi_1) \\
 x_2(t) = A_2 \cos(\omega_2 t + \phi_2)
 \end{array}
 \begin{array}{c}
 \longrightarrow \\
 \longrightarrow
 \end{array}
 \begin{array}{c}
 \boxed{S} \\
 \\
 \boxed{S}
 \end{array}
 \begin{array}{l}
 \longrightarrow y(t) = \mathcal{S}[x_1, x_2] = x_1(t)x_2(t) = \\
 = \frac{A_1 A_2}{2} \left( \cos((\omega_1 + \omega_2)t + \phi_1 + \phi_2) + \right. \\
 \left. + \cos((\omega_1 - \omega_2)t + \phi_1 - \phi_2) \right)
 \end{array}
 \quad (3.11)$$

If the input signals have a zero frequency component other combinations of the  $\omega_1$  and  $\omega_2$  frequencies will occur. However, there are so called balanced mixers that get rid of the zero frequency components and thus the unwanted output frequencies.

## 3.2 Theory of Modulation Systems

The setups of modulation systems discussed here are described mostly with phase measurements in mind rather than measurements of the signal amplitudes. This is because phase is a more delicate thing to measure. The phase measurements alone are sufficient to decide the absorption and scattering coefficients, and because amplitudes get disturbed by background light whereas the phases are not [4].

### 3.2.1 Homodyne Modulation Systems

A homodyne modulation system detects the phase shift at the radio frequency (rf) with which the light source is modulated. This is the simplest type of phase detection system because of the few components needed. However, it is also the least dynamic system, since the frequency is limited by how fast the phase detector is. In Fig. 3.7 the schematics of a homodyne system is shown.

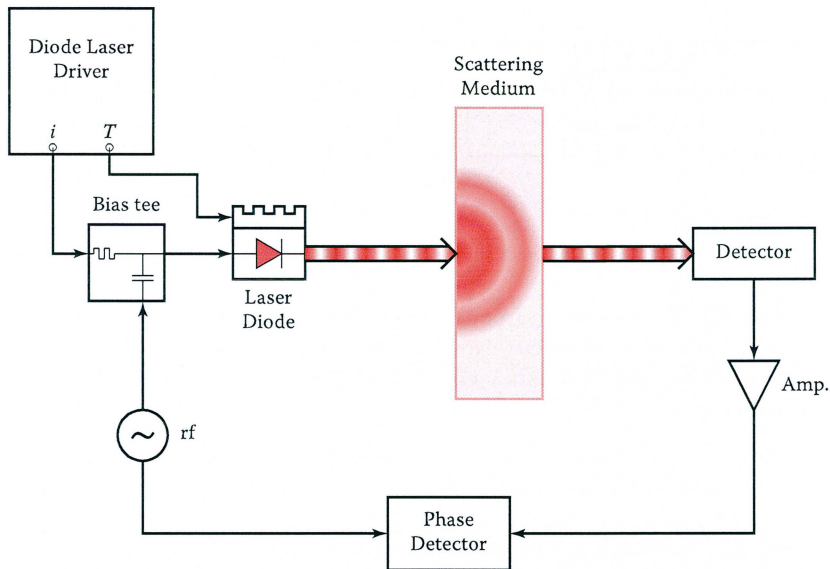


Figure 3.7: A homodyne modulation system for light measurements in a scattering medium.

The radio frequency signal is biased with the current from the diode laser driver using a bias tee. This output current is then modulating the laser diode. The amplitude modulated light emerging from the laser is then sent through a scattering medium, which adds a phase shift, and is detected with a suitable detector. The signal from the detector gets amplified before it is phase compared with the signal from the radio frequency generator. The mathematical representation of the system is shown in Fig. 3.8.

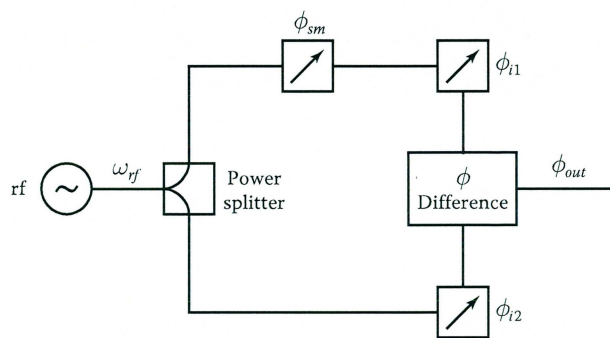


Figure 3.8: The mathematical representation of a homodyne system.

The sinusoidal signal from the frequency generator is divided into two equal parts. One is used as a reference signal and the other is the measurement signal. The latter is phase shifted with  $\phi_{sm}$  because of the medium and both signals get unwanted internal phase shifts  $\phi_i$ . These different  $\phi_i$  come from most system components, e.g. cables, circuits and photo detector, and they are highly dependent of what radio frequency  $\omega_{rf}$  is being used. The resulting phase detected is thus

$$\phi_{out} = \phi_{sm} + \sum \phi_i + \phi_{noise} \quad (3.12)$$

taking also the phase noise into account. The internal phase factors can be eliminated by initially running a phase measurement without the scattering medium and subtracting this term from the latter measured phase.

### 3.2.2 Heterodyne Modulation Systems

A heterodyne modulation system differs from a homodyne in the sense that it shifts down the radio frequency, with which the light is modulated, to a lower frequency before measuring the phase. The advantage of this is that the accuracy of the measurement is higher at lower frequencies. As shown later the phase shift due to the scattering medium is the same at the high modulation frequency as at the down converted frequency. Figure 3.9 illustrates the principles of a heterodyne modulation system.

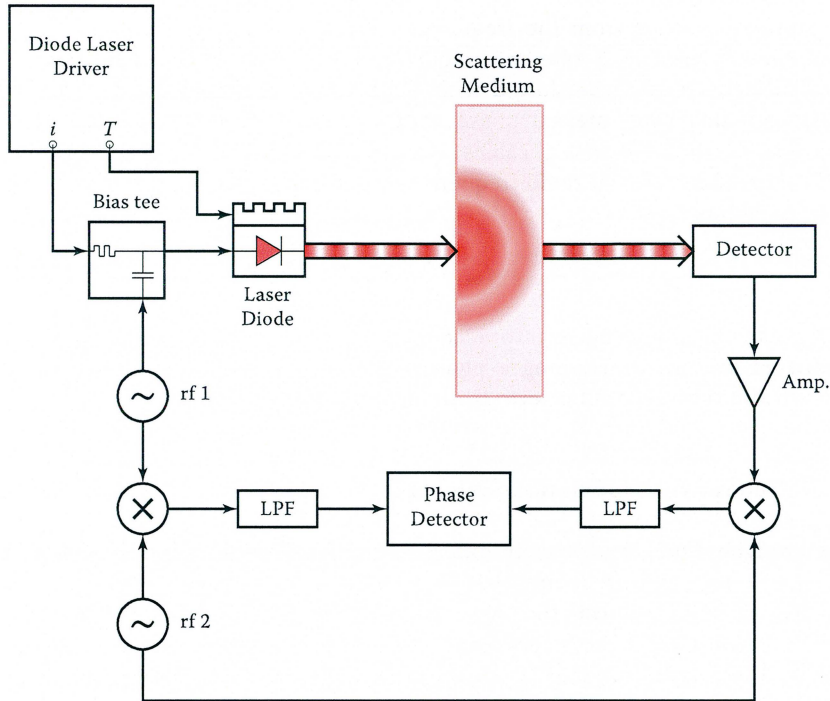


Figure 3.9: A heterodyne modulation system for light measurements on a scattering medium.

The modulation of the light is identical to the one in the homodyne method. Instead it is the reference that differs. The signal from the first radio frequency source is mixed with a signal from another source. This creates a signal going in to the middle branch containing both the sum and the difference of the radio frequencies. This signal is then filtered with a low pass filter, allowing only the difference frequency to pass and this is used as the reference. The same is done on the detection side. The amplified signal from the photo detector is mixed with the signal from the second radio frequency source, creating a frequency sum and difference. Again the difference frequency is chosen with a low pass filter. This signal and the reference are used as inputs to the phase detector to decide the resulting phase. The signal transformations in a heterodyne system are outlined in Fig. 3.10.

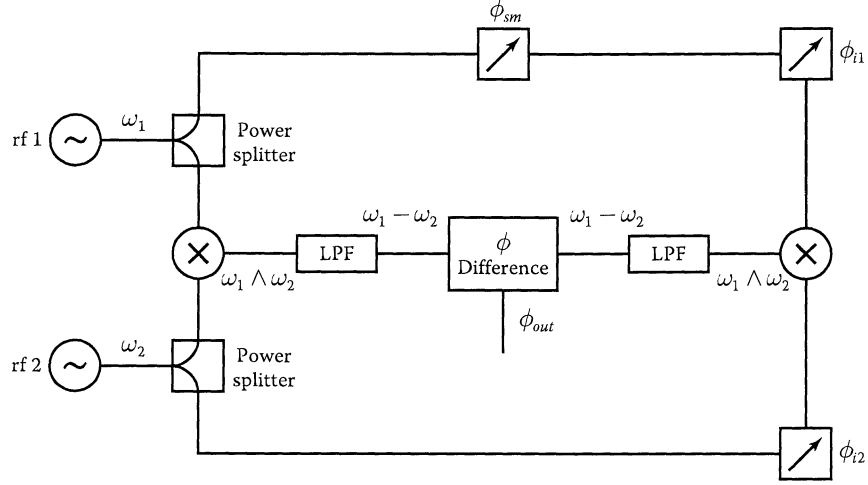


Figure 3.10: The mathematical representation of a heterodyne modulation system.

The sinusoidal signal from the first radio frequency generator gets, as in the homodyne case, the phase shifts  $\phi_{sm}$  and  $\phi_i$ . Before the mixer on the detection side, it can be written as

$$x_1(t) = A \cos(\omega_1 t + \phi_{sm} + \phi_{i1} + \phi_{noise}) \quad (3.13)$$

and the reference signal entering the mixer from below

$$x_2(t) = B \cos(\omega_2 t + \phi_{i2} + \phi_{noise}). \quad (3.14)$$

The DC components, if any exist, do not need to be taken into the equations under the assumption that the mixers are balanced. The output from the mixer to the right, will now be

$$\begin{aligned} x_{right}(t) &= x_1(t) \cdot x_2(t) = \\ &= A \cos(\omega_1 t + \phi_{sm} + \phi_{i1} + \phi_{noise}) \cdot B \cos(\omega_2 t + \phi_{i2} + \phi_{noise}) = \\ &= \frac{AB}{2} \left( \cos((\omega_1 + \omega_2)t + \phi_{sm} + \sum_1 \phi_i + \phi_{noise}) + \right. \\ &\quad \left. + \cos((\omega_1 - \omega_2)t + \phi_{sm} + \sum_2 \phi_i + \phi_{noise}) \right) \end{aligned} \quad (3.15)$$



After the low pass filter has eliminated the higher frequency, the result is

$$x_{LPF[right]}(t) = \frac{AB}{2} \left( \cos \left( (\omega_1 - \omega_2)t + \phi_{sm} + \sum_2 \phi_i + \phi_{noise} \right) \right). \quad (3.16)$$

Likewise, the signal coming from the left, looks like

$$x_{LPF[right]}(t) = \frac{A_0B}{2} \left( \cos \left( (\omega_1 - \omega_2)t + \phi_{noise} \right) \right). \quad (3.17)$$

The phase difference between the left and right signal will then be

$$\phi_{out} = \phi_{sm} + \sum \phi_i + \phi_{noise}. \quad (3.18)$$

### 3.2.3 Single Side Band Modulation Systems

When a mixer combines a radio frequency with a low or intermediate frequency, the sum and difference frequencies are called the upper and lower side band, respectively, to the radio frequency.

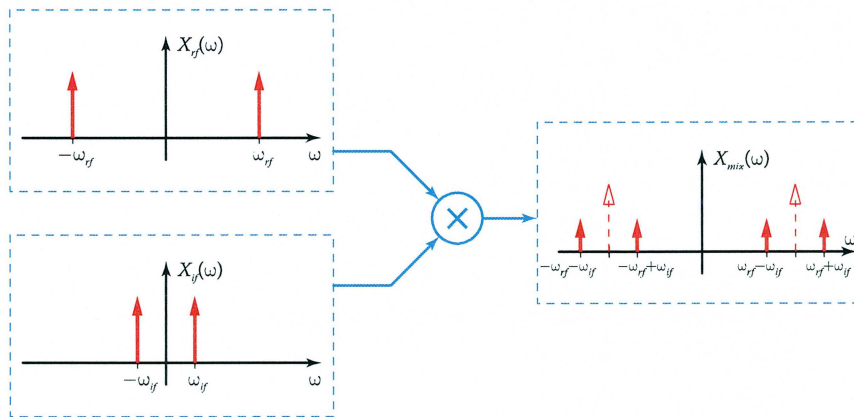


Figure 3.11: The creation of upper and lower side bands with a mixer.

A single side band (SSB) modulation system chooses one of these either with selective filtering or preferably with some more efficient method, e.g. the Hilbert transform technique described below. The advantages of using a SSB system instead of a heterodyne system is that all of the signal power is used for detection of the phase, nothing is filtered away, and that a more economic frequency generator in the audio range can be used instead of a second high frequency



generator.

Simplified one can say that a SSB system uses an intermediate frequency for detecting the phase shift springing from the shift in a much higher frequency.

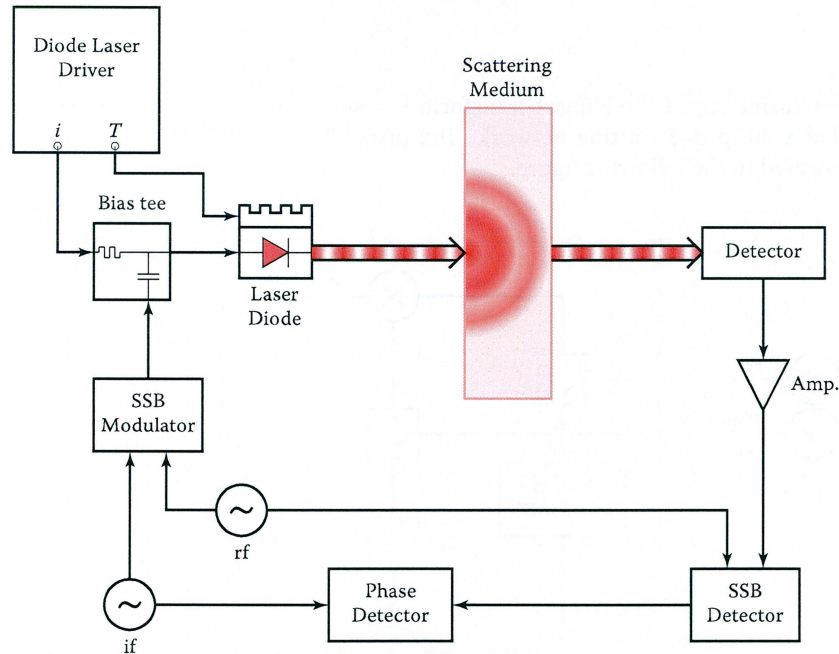


Figure 3.12: A SSB modulation system used for light measurements on a scattering medium.

The signal from the intermediate frequency source, denoted  $if$ , is in the SSB modulator combined with the signal from the radio frequency source. The SSB modulator creates a pure sinusoidal signal, if the signals from the frequency sources are sinusoidal, with a frequency of either the sum or the difference of the input frequencies. This signal gets, as before, a phase shift from the medium and from the system itself. Finally, the signal is down converted to the intermediate frequency and compared with the direct signal from the intermediate frequency source.

One way of making a SSB modulator is to utilise the properties of the Hilbert transform. A Hilbert transformer is then a filter with the impulse response

$$h(t) = \frac{1}{\pi t} \quad (3.19)$$

which in the frequency domain looks like

$$H(\omega) = \mathcal{F}[h(t)] = \begin{cases} i, & \omega < 0 \\ 0, & \omega = 0 \\ -i, & \omega > 0 \end{cases} \quad (3.20)$$

For a cosine signal the Hilbert transform is a sine. This is why it is sometimes called a 90° phase shifting network. The principles of the SSB modulator are illustrated in the following figure.

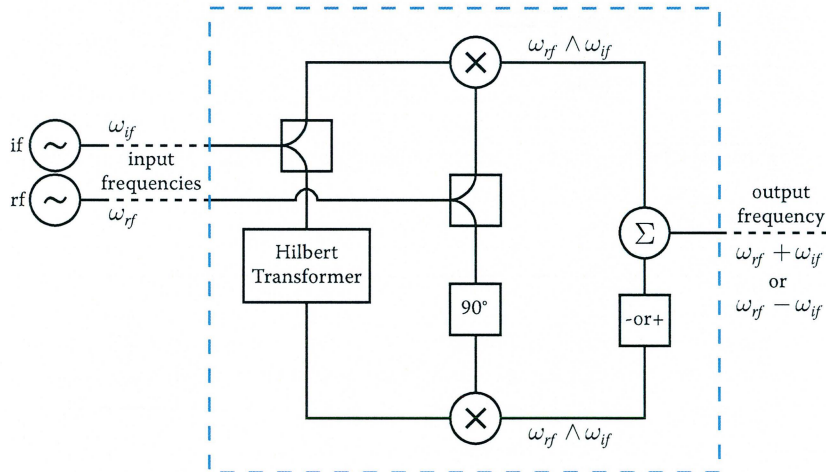


Figure 3.13: The creation of SSB signals using a Hilbert transformer.

The signals from the intermediate and radio frequency sources are the inputs to the SSB modulator. They are then divided. The signals going up are mixed as they are, and the ones going down are shifted by 90°. If pure cosine signals are used as inputs the down going signals will become sine. These are then mixed as well, and both mixed signals are combined with a power combiner, e.g. a power splitter used in the other direction, here marked with a  $\Sigma$ . If the lower signal first is negated the upper side band will be created, otherwise the lower side band is created. Mathematically the process is as follows. The output from the top and bottom mixer will be

$$\begin{aligned} x_{upper}(t) &= \frac{AB}{2} \cos(\omega_{if}t + \phi_{if}) \cos(\omega_{rf}t + \phi_{rf}), \\ x_{lower}(t) &= \frac{AB}{2} \sin(\omega_{if}t + \phi_{if}) \sin(\omega_{rf}t + \phi_{rf}). \end{aligned} \quad (3.21)$$

With these signals added together the output from the SSB modulator will be

$$\begin{aligned}
 x_{out}(t) &= \frac{AB}{2} \cos(\omega_{if}t + \phi_{if}) \cdot \cos(\omega_{rf}t + \phi_{rf}) \mp \\
 &\quad \mp \frac{AB}{2} \sin(\omega_{if}t + \phi_{if}) \cdot \sin(\omega_{rf}t + \phi_{rf}) = \\
 &= \frac{AB}{2} \cos\left((\omega_{rf} \pm \omega_{if})t + \phi_{rf} \pm \phi_{if}\right)
 \end{aligned} \tag{3.22}$$

As can be seen all of the signal power is transferred to one of the side bands. The SSB demodulator is made with a similar setup of components but shifting the sign before the power combiner. This will result in a signal with the frequency  $\omega_{if}$ . The phase shift  $\phi_{sm}$  will stay the same just as in the two other modulation systems.

## 4. Light Propagation in Scattering Media

The behaviour of light is much more complicated when inside a scattering medium than in free air. The concept of beams of light is no longer relevant because of the chaotic propagation of the photons. Instead one must refer to such approximations as the diffusion model for light transport.

Before dealing with the more complex light propagation in a medium where the scattering probability is much larger than the absorption probability, it is necessary to understand the fundamental dynamics such as reflection, absorption and scattering.

### 4.1 Fundamental Interactions of Light and Matter

When inside matter, light may be subjected to mainly three phenomena that either alters its direction or simply eradicates it. These three are, reflection against a surface, scattering and absorption. Both scattering and absorption are highly wavelength dependent.

#### 4.1.1 Reflection

Reflection is a possibility when the light hits a surface that divides materials with different refractive indices,  $n$ . The ratio between the incident and reflected power of the light is given by

$$\begin{aligned} R_{\perp} &= \left( \frac{n_1 \cos \theta_1 - n_2 \cos \theta_2}{n_1 \cos \theta_1 + n_2 \cos \theta_2} \right)^2 \\ R_{\parallel} &= \left( \frac{n_2 \cos \theta_1 - n_1 \cos \theta_2}{n_2 \cos \theta_1 + n_1 \cos \theta_2} \right)^2 \end{aligned} \tag{4.1}$$

where  $R_{\perp}$  and  $R_{\parallel}$  are the reflectances for light polarized perpendicularly and parallel to the incident plane, respectively. The refractive indices of the materials

are denoted  $n_1$  and  $n_2$ . The angle of incidence,  $\theta_1$ , and the angle of transmission,  $\theta_2$ , are given by the Snell law:

$$n_1 \sin \theta_1 = n_2 \sin \theta_2 \quad (4.2)$$

#### 4.1.2 Absorption

The probability of light getting absorbed by a material is given by the absorption coefficient,  $\mu_a$  per unit length. When the absorption coefficient is dominant over the scattering coefficient, defined below, the absorption of light is described by the Beer-Lambert law

$$I(\nu, x) = I_0 \exp(-\mu_a(\nu) \cdot x) \quad (4.3)$$

This describes the recorded intensity  $I$  at a frequency  $\nu$  to be decreased exponentially from the original intensity  $I_0$ . The absorbing path length is denoted  $x$ .

#### 4.1.3 Scattering

Photons can, when passing through a material, get disturbed by the particles in the material so that their direction is changed. This phenomenon is called scattering. In cases with small scattering particles, in relation to the wavelength of the light, scattering is divided into Rayleigh and Raman scattering. Rayleigh scattering is an elastic process, i.e. the scattered photon energy is preserved, while in the latter case its energy is diminished. The scattering probability is proportional to  $1/\lambda^4$ .

For larger scattering objects, Mie scattering can occur. This is an elastic process like Rayleigh scattering, but the scattering cross section is more complicated and varies also with object size, refractive indices and absorption.

The scattering coefficient,  $\mu_s$  per unit length, is the probability of light being scattered. However, scattering does not need to be an isotropic process. Therefore a reduced scattering coefficient is introduced,  $\mu'_s$ , which is

$$\mu'_s = \mu_s (1 - \bar{p}) \quad (4.4)$$

where  $\bar{p}$  is the average cosine of the scattering angle or the anisotropy factor, sometimes called  $g$ . A  $\bar{p}$  close to zero indicates a nearly isotropic scattering, while the scattering is mostly directed forward if  $\bar{p}$  is close to one.

## 4.2 Light Transport Theory

If light is sent into a highly scattering medium, then the light detected somewhere else will have travelled a significantly longer way than the distance between the input and output. Since the scattering coefficient is much larger than the absorption coefficient in these materials, the Beer-Lambert law is not directly applicable. For quantitative measurements, it is necessary to decide how much longer this path length is. Analytical expressions to calculate this path length have been derived by, for example, Arridge *et al.* [5], which are the basis for the calculations that follows in this chapter.

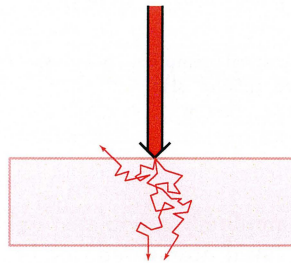


Figure 4.2: Light paths in a scattering medium.

Instead of building a model of how the light propagates in a scattering medium with the Maxwell equations, which would be a much too extensive task since most of the media are microscopically inhomogeneous, one has to make certain approximations. The transport theory, for example, treats the problem as a transport of energy and thus neglects phenomena like diffraction and interference. The light propagation can be calculated either by Monte Carlo simulations or by solving the transport equations. [6-8]

### 4.2.1 Time and Frequency Domain Solutions

If a very short pulse, a few picoseconds long, of light is sent into a scattering medium, a much smaller pulse followed by a broad distribution of light can be observed, if measured on the transillumination side; see Fig. 4.3. The first pulse consists of the few ballistic photons that have remained unscattered and the distribution consist of the photons that have been scattered. The curve can be interpreted as a distribution of arrival times or path lengths and is called the temporal point spread function (TPSF). The TPSF is the light impulse response of the medium and is written as a Green's function,  $g(t)$ . The mean path length is equal to the speed of light times the mean time

$$\langle l \rangle = c \langle t \rangle. \quad (4.5)$$



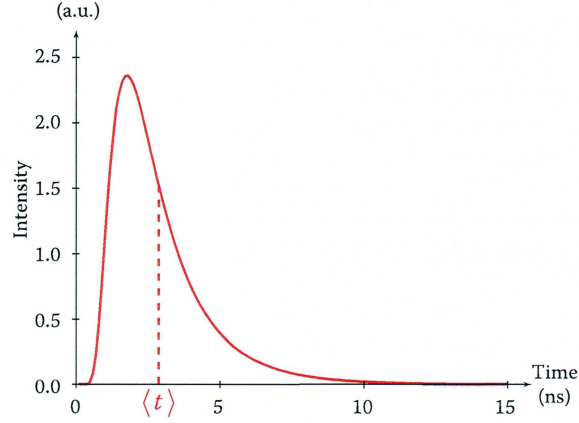


Figure 4.3: Theoretical temporal point spread function for a transilluminated infinite slab with a thickness of 2.95 cm,  $\mu_s = 3100 \text{ m}^{-1}$  and  $\mu_a = 0.31 \text{ m}^{-1}$

If instead sinusoidally, amplitude modulated light is sent into the medium the light will as before be delayed, attenuated, and broadened in time because of the scattering. This will result in a phase shift and a decreased modulation. Since the modulated light and the pulse of light are each others Fourier transform, the output in the modulation case will be a Green's function in the frequency domain,  $G(\omega)$ .

The intensity of the light sent into the medium is written as

$$x_{in}(t) = (A + B \cos(\omega_m t)) \cos(\omega_c t) \quad (4.6)$$

where  $\omega_c$  and  $\omega_m$  are the angular frequencies of the light itself and of the modulation. A and B are constants. Since the detector is not capable of detecting the fast oscillation of the light itself, the last cosine term can be disregarded. From the previous chapter we know that the output from a system is the convolution of the impulse response and the input signal. (Please note that the convolutions and Fourier transforms here following has a different normalization than used elsewhere, in order to match the formulae given by Arridge *et al.* [5])

$$\begin{aligned} x_{out}(t) &= g(t) * x_{in}(t) = \frac{1}{\sqrt{2\pi}} \int_{-\infty}^{\infty} x_{in}(t-t') g(t') dt' = \\ &= A \frac{1}{\sqrt{2\pi}} \int_{-\infty}^{\infty} g(t') dt' + B \frac{1}{\sqrt{2\pi}} \int_{-\infty}^{\infty} \cos(\omega_m(t-t')) g(t') dt' = \\ &= AG(0) + B \frac{1}{\sqrt{2\pi}} \int_{-\infty}^{\infty} \frac{1}{2} (e^{i\omega_m(t-t')} + e^{-i\omega_m(t-t')}) g(t') dt' = \\ &= AG(0) + B \frac{1}{2} (e^{i\omega_m t} G(\omega_m) + e^{-i\omega_m t} G(-\omega_m)). \end{aligned} \quad (4.7)$$

But since  $g(t)$  is a real function the solution can be made simpler:

$$\begin{aligned} g(t) \in \mathbb{R} &\Rightarrow G(-\omega_m) = G^*(\omega_m) \\ \Leftrightarrow x_{out}(t) &= AG(0) + B \cdot |G(\omega_m)| \cdot \cos(\omega_m t + \arg(G(\omega_m))). \end{aligned} \quad (4.8)$$

This equation show that the signal zero frequency component is decreased with  $G(0)$ , the modulation with the absolute value of the Fourier transformed Green's function at the frequency  $\omega_m$ , and that the signal phase is retarded by the argument of  $G(\omega_m)$ .

If the Green's function is known then the mean time delay can be calculated. This mean time, or average time of flight, is the weighted mean of the TPSF

$$\langle t \rangle = \frac{\int_{-\infty}^{\infty} g(t) t dt}{\int_{-\infty}^{\infty} g(t) dt} \quad (4.9)$$

or in the frequency domain

$$\langle t \rangle = i \frac{\left. \frac{\partial}{\partial \omega} G(\omega) \right|_{\omega=0}}{\left. G(\omega) \right|_{\omega=0}}. \quad (4.10)$$

#### 4.2.2 Diffusion Model for Light Transport

When having the tools to decide the phase shift and the mean time from the Green's function, it is possible to link them together if the shape of this Green's function is known. The Green's function can be found by solving the diffusion equations for light transport in different geometries. The procedure of using the diffusion equations is today accepted as a reliable model for these calculations [9].

The so called time dependent  $P_1$  approximation to the transport equation states that

$$\left( \nabla \cdot \gamma^2 \nabla - \mu_a c - \frac{\partial}{\partial t} \right) \Phi(\mathbf{r}, t) = -q(\mathbf{r}, t). \quad (4.11)$$

Here  $\Phi$  is the desired photon density,  $\mu_a$  the absorption coefficient,  $c$  the velocity of light,  $q$  the term from the input source and  $\gamma$  is

$$\gamma^2 = c \left/ \left( 3 \left( \mu_a + (1 - \bar{p}) \mu_s \right) \right) \right. \quad (4.12)$$



In the case of an isotropic medium Eq. 4.11 can be written

$$\left( \gamma^2 \nabla^2 - \mu_a c - \frac{\partial}{\partial t} \right) \Phi(\mathbf{r}, t) = -q(\mathbf{r}, t). \quad (4.13)$$

If the photon density is scaled by the photon energy, the gradient of  $\Phi$  corresponds to an intensity. The intensity  $x_{out}(t)$  can be derived from the solution of  $\Phi$  in a volume  $\Omega$  bounded by  $\partial\Omega$ .

$$\Gamma(\boldsymbol{\xi}, t) = -\gamma^2 \frac{\partial}{\partial \mathbf{n}} \Phi(\mathbf{r}, t) \Big|_{\partial\Omega} = -\gamma^2 \hat{\mathbf{n}} \cdot \nabla \Phi(\mathbf{r}, t) \Big|_{\partial\Omega} \quad (4.14)$$

In this equation  $\Gamma(\boldsymbol{\xi}, t)$  corresponds to  $x_{out}$ . However, it is defined with a positive frequency complex exponential instead of a cosine function. The outward surface normal is denoted  $\hat{\mathbf{n}}$  and  $\boldsymbol{\xi}$  is a point on the boundary. The solutions for several geometries given by Arridge *et al.* can be found in Appendix A [5].

## 5. Gas in Scattering Media Absorption Spectroscopy (GASMAS)

Scattering media, such as porous solids or turbid liquids, are likely to contain different free gases. This is the case in both organic and synthetic materials, e.g. plants, tissue, stones, ceramics, powders, etc. To spectroscopically detect and characterise gases in these materials, one cannot straightforwardly apply the Beer-Lambert law because of the unknown path lengths, as described in the previous chapter. By a technique, denoted **gas in scattering media absorption spectroscopy (GASMAS)**, it is possible to measure these gases. This technique uses the fact that the absorption features of the gases are much narrower than the relatively slow changes in absorption in the bulk material.

### 5.1 Absorption Spectroscopy

Absorption spectroscopy is used to determine concentration, temperature and pressure of gases. By using tuneable lasers, these properties can be measured to a very high accuracy and precision. The requirement is that a valid theoretical model describing the absorption lines, under the measurement conditions, is available. The absorption lines in the oxygen A-band can be seen in Fig. 5.1. The Beer-Lambert law, see Eq. 4.3, is the bedrock of all absorption measurements. Since the absorption coefficient is a product between the absorption cross-section and the concentration of absorbing molecules, the concentration can be determined if this cross-section is known. The cross-section itself is a function of the line shape, which depends on both the pressure and the temperature of the gas. With knowledge about these dependencies, the temperature and pressure can be calculated [10].

#### 5.1.2 Wavelength Modulation

In wavelength modulation (WM), a small sinusoidal modulation is superimposed on the current controlling the laser. The frequency of this modulation is quite low, in the order of 1-100 kHz, compared to the line width of the absorption line,

which is in the GHz range. This frequency is also sent to a lock-in amplifier and is used as the reference signal. The signal from the photo detector is compared with the reference in the lock-in amplifier. The result from the lock-in amplifier will resemble the derivative of the direct signal from the photo detector. If the lock-in instead is operated at the second harmonic of the modulation frequency, i.e. double the frequency, the result will be the second derivative of the direct signal. This is also the most frequent way of detection. The detection limit of wavelength modulation spectroscopy (WMS) is usually about  $10^{-5}$  but lower limits are possible [3, 11].

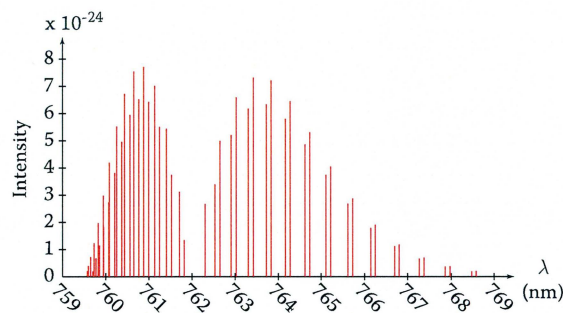


Figure 5.1: Absorption lines in the oxygen A-band [12].

## 5.2 The GASMAS Method

Simplified, one can say that the GASMAS method uses a WM technique to measure the absorption over one or several absorption lines of a free gas contained in a scattering medium. The concentration of the gas can be determined either in relation to another gas concentration or with a theoretical model of the optical path length. The GASMAS method was first demonstrated in 2001 by qualitatively monitoring free oxygen [13]. Later, quantitative measurements [14] and measurements on wooden materials have been demonstrated [15].

### 5.2.1 The GASMAS Setup

The temperature controlling the laser diode wavelength is changed, so that the wavelength of the light is close to an absorption line of the gas in question. By applying a ramp to the current controlling the diode laser, the laser's wavelength is swept over one or several absorption lines. The intensity of the signal detected, the direct signal, will have the ramp shape of the input current. The ramp will also exhibit a small dip, due to the increased absorption at the absorption line of the gas. Wavelength modulation is used to increase the visibility of this dip. As described above, the second harmonic of the direct signal will resemble the

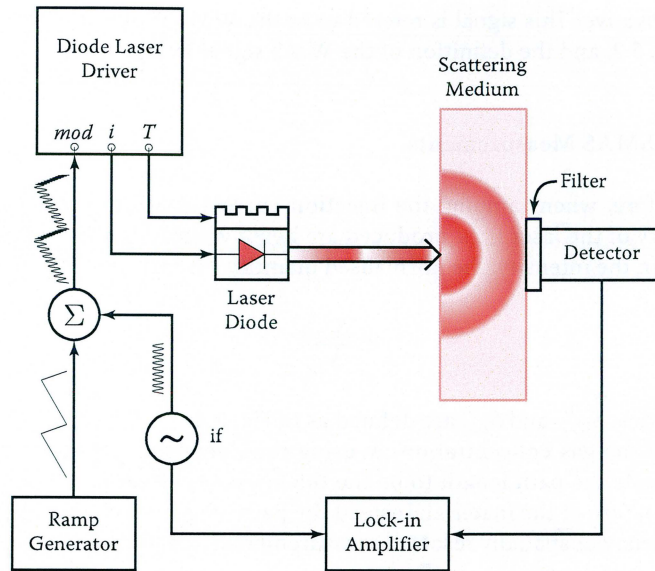


Figure 5.2: The setup of a GASMAS system for transillumination measurement on a gas in a scattering medium.

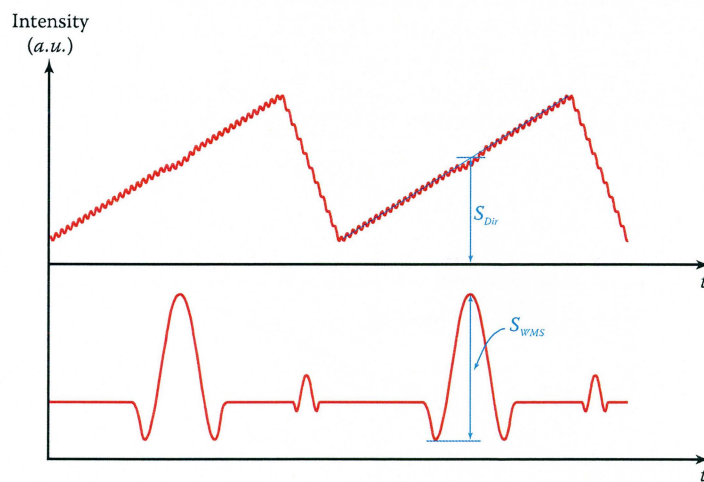


Figure 5.3: Schematic direct signal and signal from the lock-in amplifier along with the definition of  $S_{Dir}$  and  $S_{WMS}$ .

second derivative. This signal is referred to as the WMS signal. The setup can be seen in Fig. 5.2, and the definition of the WMS signal in Fig. 5.3.

### 5.2.2 GASMAS Measurements

As said before, when ramping the injection current, both the wavelength and the intensity of the laser light produced are being varied. To compensate for the variations in the intensity, the normalised quantity  $g$  is introduced

$$g \equiv \frac{S_{WMS}}{S_{Dir}}, \quad (5.1)$$

The quantities,  $S_{WMS}$  and  $S_{Dir}$ , are defined as in Fig. 5.3.

To find the gas concentration by using the Beer-Lambert law, one cannot simply assume the path length to be the thickness of the sample because of the scattering nature of the material. Instead the path length must be evaluated with time, frequency or spatially resolved measurements, as described in chapter four. The optical path length,  $L_{sm}$ , is thus

$$L_{sm} = \langle l \rangle = v \langle t \rangle, \quad (5.2)$$

where  $v$  is the velocity of light in the scattering medium. The average time of flight for the chosen geometry can be found in Appendix A. However, one can calculate an equivalent mean path length,  $L_{eq}$ , which corresponds to the distance the light would have travelled in a certain atmosphere to get the equal signal. In the case of oxygen this can be done by adding small columns of air and measure the effect on the signal,  $g$ . The equivalent mean path length is then found by extrapolating the line on which the signals lie. This method is called the standard addition method and is illustrated in the following figure.

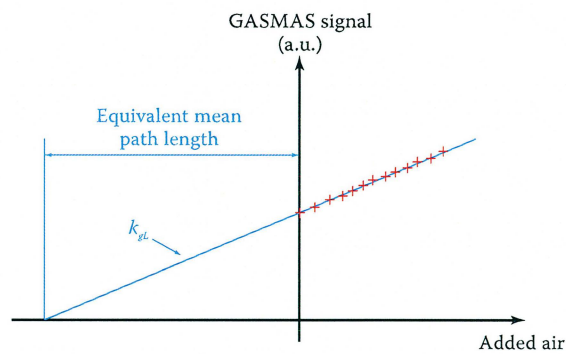


Figure 5.4: A schematic picture of the standard addition method showing how the equivalent mean path length and the slope  $k_{gL}$  can be evaluated by extrapolation of line on which the GASMAS signals lie.

If the optical path length is known then the concentration of gas inside the scattering medium,  $c_{sm}$ , can be determined by

$$c_{sm} = \frac{c_{atm} L_{eq}}{L_{sm}} = \frac{g}{L_{sm}} \frac{c_{atm}}{k_{gL}}. \quad (5.3)$$

The concentration  $c_{atm}$  is the concentration of the gas in the surrounding atmosphere and  $k_{gL}$  is the slope of the extrapolated line in Fig. 5.4. The porosity of the medium,  $P$ , can be defined as

$$P \equiv \frac{c_{sm}}{c_{atm}} \quad (5.4)$$

if there is gas equilibrium with the surrounding atmosphere. The index of refraction of the scattering medium can, by the aid of the porosity, be estimated to

$$n_{sm} = P n_{air} + (1 - P) n_b, \quad (5.5)$$

where  $n_{air}$  and  $n_b$  are the indices of the air and the bulk material, respectively. The index of refraction of the scattering medium is required to decide the speed of light inside the medium [14].

If a material is stored in a different atmosphere, not containing the gas under study, the reinvasion rate of the gas can easily be evaluated with the GASMAS method. When the material is taken out of the different atmosphere, the quantity  $g$  is measured over time. The rate by which  $g$  increases is the rate of the gas reinvasion since  $g$  is proportional to the gas concentration (Eq. 5.3). GASMAS may also be a tool for determining the moisture level in a material by, the absence of, e.g., oxygen rather than the presence. Other applications could be gas tomography. This requires a development of an imaging GASMAS system. The advantage of using spectroscopic methods is that it is non-invasive and thus has a minimal effect on the materials [14].

## 6. Diagnostics of Laser Diodes

The most essential device in GASMAS measurements is the laser diode. It has to have a wavelength characteristic that covers at least one absorption line, and that is continuous in the vicinity of that line. The diodes that were evaluated for use in the new GASMAS setup were several newly purchased diodes from Roithner Lasertechnik and one from SHARP. All of the lasers were supposed to be able to reach the oxygen A-band at around 760 nm, see Fig. 5.1.

### 6.1 Diagnostical Setup and Method

The SHARP diode (SHARP LT031MDO 0-30) was the most thoroughly examined one. The output power was measured as a function of the operation current at the temperature 30 °C. The operation current needed for a low and a high output power was measured as a function of temperature. Finally, the wavelength was tuned with the temperature to search for oxygen absorption lines and mode jumps. The threshold current and wavelength of the Roithner diodes were only briefly examined.

#### 6.1.1 SHARP Laser Diode LT031MDO 0-30

The SHARP diode was placed in a THORLABS diode holder. The current and temperature were controlled by a Melles Griot 06DLD203A laser driver. According to the specifications of the diode, the peak power was 10 mW, the nominal wavelength 757 nm, and the threshold current 34 mA. For power measurements, an optical power meter from THORLABS was used. Initially, the temperature was set to 30 °C. The output power was measured directly after the diode for operation currents between 25 and 49 mA in steps of 1 mA. The power meter was slightly tilted to avoid back reflections from its surface. The power after the collimating lens was occasionally measured as well.

In order to find guidelines for the limits of the operation current at different temperatures, both a low and a high power value was chosen. To ensure that the peak power of the laser was not exceeded, the high power measured after the collimation lens,  $P_{high}$ , was chosen to 6.1 mW. This represents a power of about

7.4 mW directly after the diode. The lower power value was chosen to 1.1 mW,  $P_{low}$ . It was also measured after the collimating lens. This value is a bit above the threshold to ensure that the light really was of laser nature. The currents,  $I_{low}$  and  $I_{high}$ , resulting in the chosen power values were measured for temperatures between 20 and 54 °C, with a change of 2 °C between the measurements. Higher temperatures were not used, in order to avoid thermal degradation of the diode laser.

Finally, absorption lines were searched with a WMS setup; see Fig. 6.1. The light was also split with a very thin glass plate, letting a small fraction of the light enter a Burleigh wave meter, so that the wavelength could be determined. The operation current was modulated with a ramp, spanning about 500 mV, and a small, superimposed sinusoidal voltage with a frequency of some tens of kilohertz. The light was detected with a photo diode. The signal was amplified with a resistor and sent to an EG&G Princeton Applied Research Model 5209 lock-in amplifier. The resulting second harmonic of the signal was shown on a Tektronix TDS 3034B oscilloscope. While the temperature was swept between 20 and 50 °C, the image on the oscilloscope was studied to see if any WMS-like signal emerged. If that was the case, the output from the Burleigh was analysed to decide whether the signal was caused by an absorption line or a mode jump.



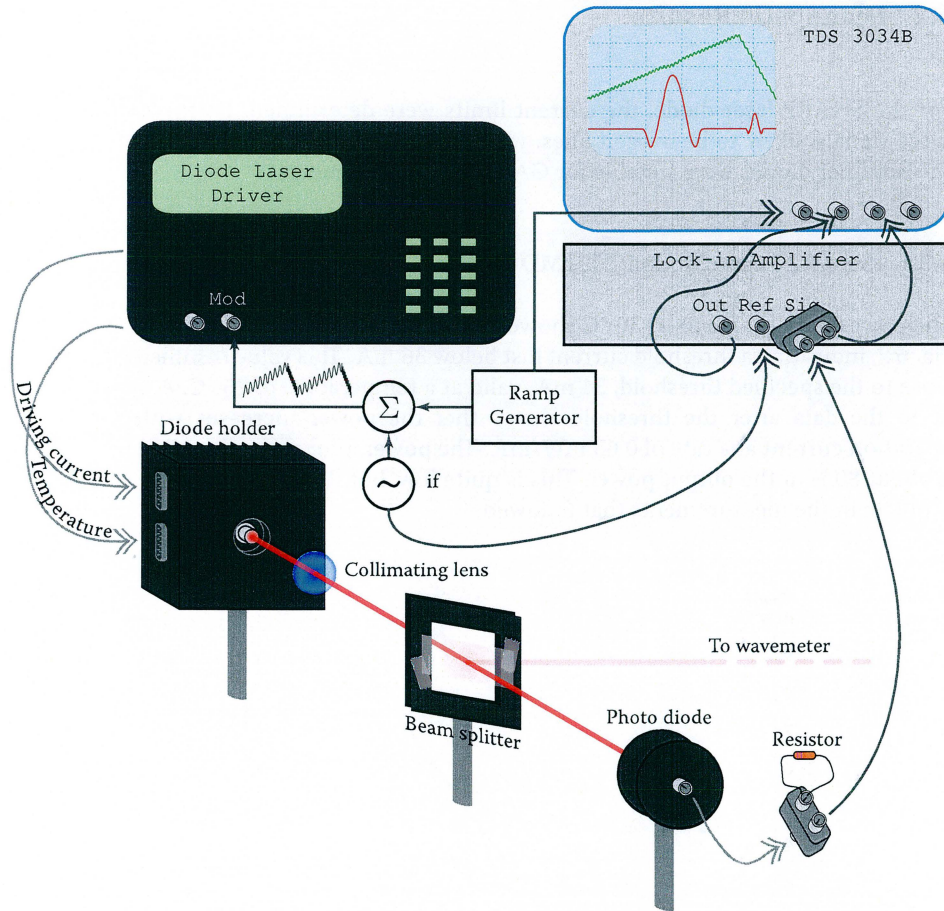


Figure 6.1: The WMS setup used to diagnose the SHARP laser diode.

### 6.1.2 Roithner Lasertechnik Laser Diodes

According to the specifications that followed with the Roithner laser diodes, their nominal wavelengths were 760 nm and the threshold current was 13 mA, at maximum 20 mA. The diodes were, one by one, placed in the diode holder. Their power were measured to see when they started to lase. The light was directed into the Burleigh wave meter to measure their wavelengths at different temperatures.

## 6.2 Diagnostic Results

For the SHARP laser diode, the current limits were determined. Furthermore, three signals, likely to be oxygen lines, were found. On the other hand, none of the Roithner diodes were suitable for GASMAS measurements.

### 6.2.1 SHARP Laser Diode LT031MDO 0-30

The power measurements at 30 °C showed a clear diode laser characteristic; see Fig. 6.2, indicating a threshold current just below 36 mA. This value is sufficiently close to the specified threshold, 34 mA, valid at a temperature of 25 °C. A linear fit to the data after the threshold shows that the power increases with the operation current at a rate of 0.63 mW/mA. The power after the collimating lens is about 80 % of the output power. This is quite low, but it is not too low to be a problem in the measurements that followed.

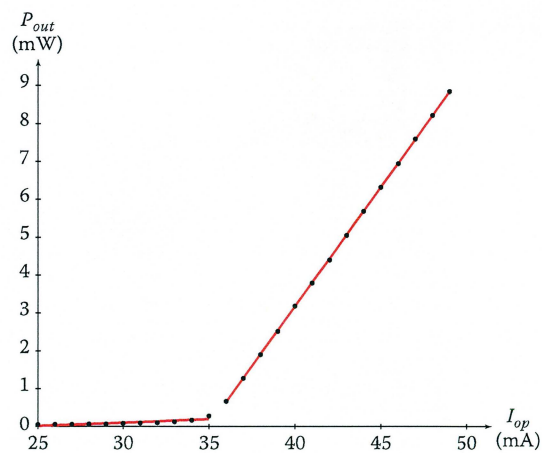


Figure 6.2: The power of the light, measured directly after the diode laser, as a function of the operation current when the diode was kept at 30 °C.

The measured operation currents needed to reach the powers  $P_{low}$  and  $P_{high}$  at different temperatures can be seen in Fig. 6.3. This shows that the current needed to reach the same power increases with  $0.2 \text{ mA}/^{\circ}\text{C}$ .

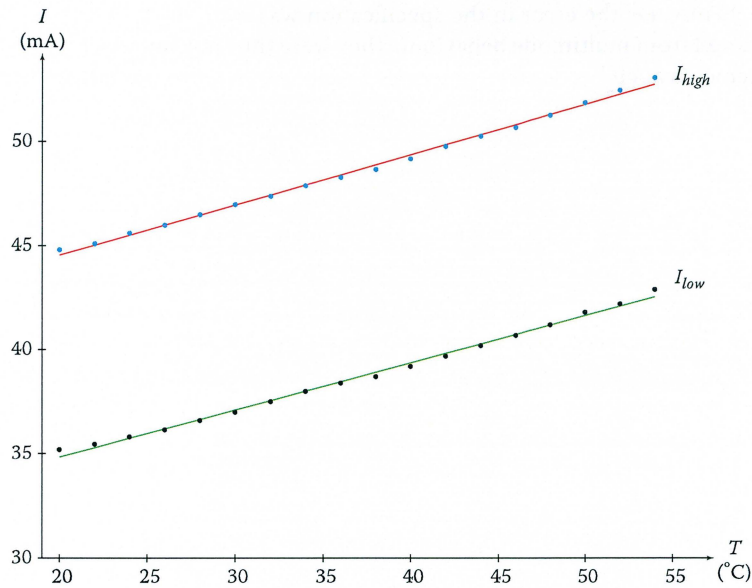


Figure 6.2: The power of the light, measured directly after the the diode laser, as a function of the operation current when the diode was kept at  $30^{\circ}\text{C}$ .

With the temperature being swept from  $20$  to  $50^{\circ}\text{C}$ , one could with the Burleigh unit see that the wavelength was well below  $760 \text{ nm}$  in the first temperature region. Since the oxygen A-band does not begin before  $759.58 \text{ nm}$ , it was not necessary to do a WMS measurement at first. Slightly below  $760 \text{ nm}$ , a highly irregular behaviour started where the modes died rapidly and were replaced by others. The temperature was now about  $43^{\circ}\text{C}$ . This behaviour stopped at  $761 \text{ nm}$  and three, well shaped WMS signals were recorded. The Burleigh wave meter showed no indication of multimode or mode jump behaviour around these signals. The wavelength was measured at the centre of these lines and was found to be  $761.26 \text{ nm}$ ,  $761.39 \text{ nm}$ , and  $761.50 \text{ nm}$ , respectively. When compared with a table over the oxygen A-lines, the lines R5R5, R3Q4, and R3R3, were probable to be the cause of the signals recorded. These three lines are consecutive and located at the wavelengths,  $761.255 \text{ nm}$ ,  $761.416 \text{ nm}$ , and  $761.529 \text{ nm}$ , respectively [12]. The wavelengths measured with the Burleigh unit can be used as a good guideline but should not be regarded as totally reliable.

As a conclusion, one could say that the SHARP diode could be very well suited for GASMAS measurements.

### **6.2.2 Roithner Lasertechnik Laser Diodes**

All of the diodes from Roithner were found to perform far from their specifications. Their wavelengths were above 770 nm, i.e. outside the oxygen A-band, even at low temperatures. The threshold currents were measured to be around 90 mA, i.e. the error in the specification was over 400 %. Many of them also suffered from multimode behaviour. They were thus not suited for GASMAS measurements at all.



## 7. Setup of a GASMAS System

Using some newly purchased equipment, a new GASMAS system was set up. The SHARP diode, examined in Chap. 6, was used as a light source. The first task was to couple the laser light into an optical fibre.

### 7.1 Fibre Coupling

The light from the laser diode, SHARP LT031MDO 0-30, was focused with a lens onto the centre of the fibre. After the fibre, the light was collimated with a collimator package. The power of the light was measured in between every step of the fibre coupling; see Fig. 7.1. The calculations in this section are based on equations that can be found in, e.g. Ref. [16].

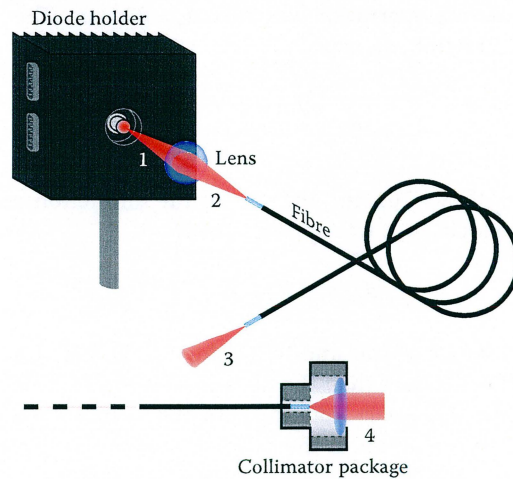
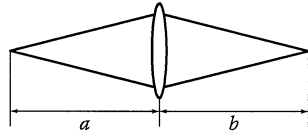


Figure 7.1: Coupling of laser light into an optical fibre. The numbers indicate positions where the optical power was measured.

The lens had a focal length of  $f = 4.5$  mm and its numerical aperture was  $NA_{lens} = 0.55$ . The lens was placed in such a position that the focal spot was minimised and had a smooth elliptic shape, just as the light directly after the diode. If the divergence angle of the laser light is assumed to be between  $30^\circ$  and  $45^\circ$ , it would represent a numerical aperture of  $NA_{laser} = 0.5 - 0.57$ . This could mean that some light is lost already between step 1 and 2. With a 1:1 imaging, the distances between the laser, lens, and focal point, should according to the thin-lens equation be



The diagram shows a thin lens with two focal points. The object distance is labeled 'a' and the image distance is labeled 'b'. The lens is represented by a vertical oval. Two lines from the top and bottom of the lens converge at a point on the right, representing the focal point. The distance from the lens to this point is 'b'. Similarly, two lines from the top and bottom of the lens diverge from a point on the left, representing the object. The distance from this point to the lens is 'a'.

$$\frac{1}{f} = \frac{1}{a} + \frac{1}{b} \Rightarrow a = b = 2f \quad (7.1)$$

There were two effects that could affect the size of the focus; aberration and diffraction. As for spherical aberration, the diameter of the focus,  $d_a$ , can be written as

$$d_a = K(n) \left( \frac{D}{f} \right)^3 \cdot b \quad (7.2)$$

where  $D$  is the diameter of the lens and  $K(n)$  is a function of the refractive index

$$K(n) = \frac{1}{128} \left( \frac{n}{n-1} \right)^2 \quad (7.3)$$

The lens was assumed to be made of BKZ glass with  $n \approx 1.52$ , and  $D \approx 5$  mm. The focal size due to spherical aberration was thus,  $d_a = 824 \mu\text{m}$ . The diameter of the focal spot due to diffraction,  $d_d$ , was

$$d_d = \frac{2 \cdot 1.22 \cdot \lambda}{D} \quad (7.4)$$

With a wavelength of,  $\lambda = 761$  nm, the size of the diffraction was  $d_d = 3.3 \mu\text{m}$ . The total size of the focus,  $d_{tot}$ , was approximately

$$d_{tot} \approx 0.83 \text{ mm}. \quad (7.5)$$

The fibre, designed for visible and NIR light, had a core diameter of  $600 \mu\text{m}$ . Since the focal spot was larger than the fibre core, it was impossible to get all of the light through the fibre. Apart from this loss, there will also be losses between step 2 and 3 due to attenuation in the fibre. The fibre numerical aperture was  $NA_{fibre} = 0.49$ .

The collimator package was a THORLABS F230SMA-B unit. It had a numerical aperture,  $NA_{collimator} = 0.55$  and a focal length of 4.5 mm. Since  $NA_{collimator} > NA_{fibre}$  there should have been no significant losses between step 3 and 4. Also, the light could be collimated.

When measuring in every step, the powers were found to be,  $P_1 = 4.1$  mW,  $P_2 = 4.1$  mW,  $P_3 = 3.4$  mW and  $P_4 = 3.3$  mW. About 80 % of the light could thus be coupled through the fibre.

## 7.2 The Setup

When the light had been coupled into the fibre a GASMAS system could be put together. The setup is illustrated in Fig. 7.2. The laser was controlled with a Melles Griot 06DLD103 diode laser driver. The ramp was produced by a Tektronix FG501A function generator, and the sinusoidal modulation by a Rhode&Schwarz SML 01 signal generator. The oscilloscope, a Tektronix TDS 520B, was triggered on a pulse signal from the function generator. The pulses had the same frequency as the ramps. The lock-in amplifier, Signal Recovery 7280 DSP, got the reference signal from the signal generator. The light was detected with a Hamamatsu R5070 photo multiplier tube (PMT). Stray light was blocked with a filter. The outgoing signal from the PMT was amplified by using a resistor of 2.2 k $\Omega$ . This direct signal was sent both to the lock-in amplifier and the oscilloscope. The ramping signal had a frequency of about 10 Hz and the sinusoidal signal had a frequency of 55 kHz.

When the temperature of the laser was 48.4 °C and the operating current at the middle of the ramp, was 45.6 mA, a GASMAS signal was obtained. The light was sent to the Burleigh wave meter. It showed no signs of multimode behaviour and had no mode jumps around the operating current. The absorption line found was thus the oxygen R3R3 line; see Sect. 6.2.1. However, the GASMAS signal had an overall wavelike behaviour. This was caused by fringes, i.e. reflections of the light between the surfaces. By vibrating both the diode holder and the plate, on which the scattering medium was placed, the fringes evened out and a signal like the one in Fig 7.3 was obtained.

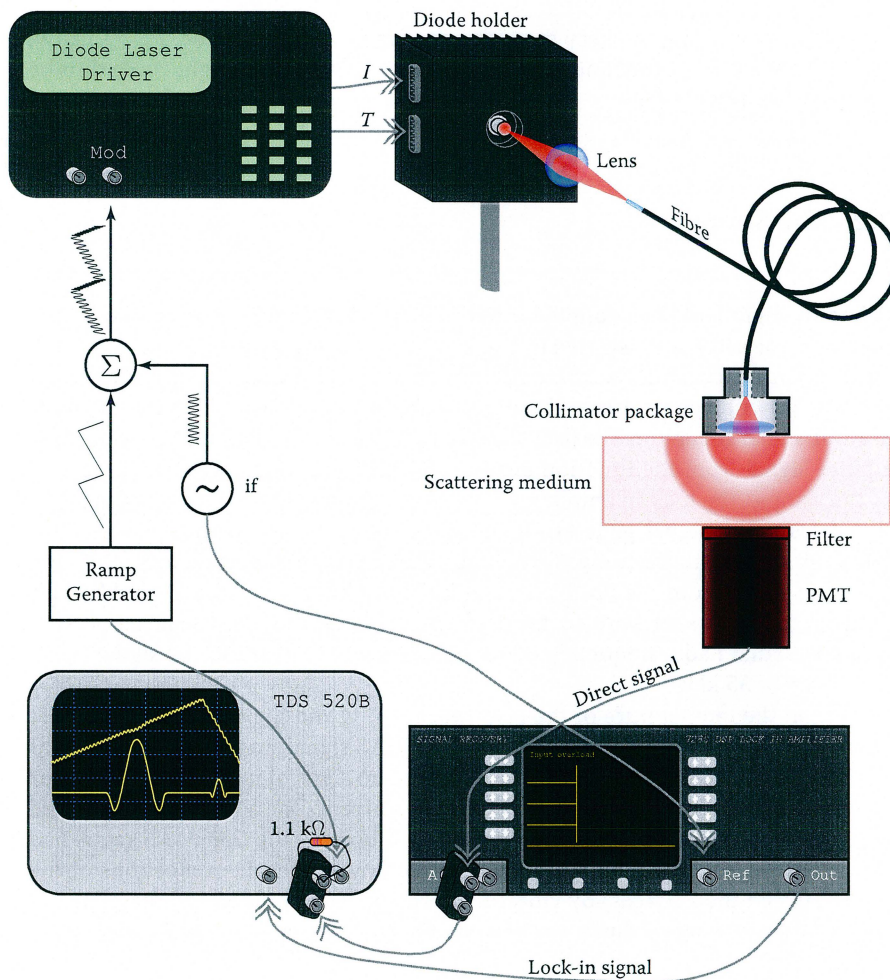


Figure 7.2: Illustration of the setup used for GASMAS measurements.



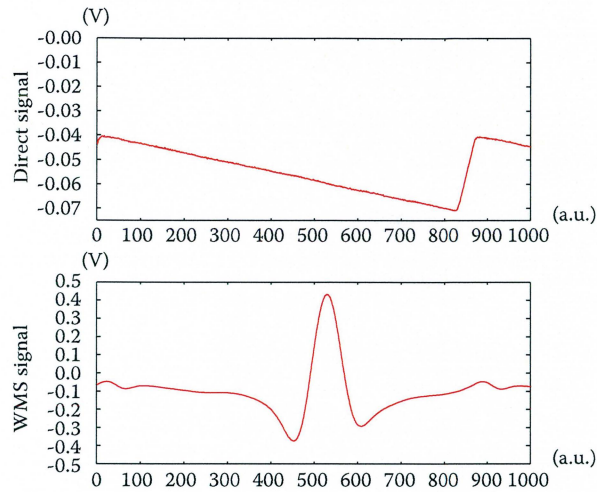


Figure 7.3: A GASMAS signal from a polystyrene foam sample, with a thickness of 17 mm.

### 7.3 Measurements on Wheat Flour

An experiment was meant to be done on wheat flour. The aim was to see how the signal changed when adding flour but keeping the sample volume constant. A cylinder with a plexiglas bottom was constructed for the experiment; Fig. 7.4.

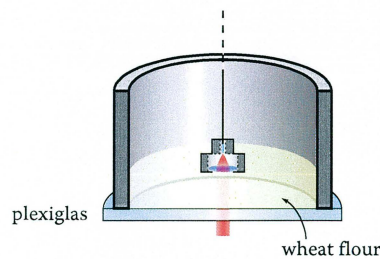


Figure 7.4: Illustration of the cylinder used for GASMAS measurements on wheat flour.

Unfortunately, this method turned out not to work to a satisfactory level. The flour was found to highly attenuate the light even for thin layers of flour,  $\sim 5$  mm. Also, difficulties arose when trying to evenly distribute the flour over the bottom surface. The third problem found, was the difficulty to compress the flour to the original level, when more was added. Improvements can probably be made by spreading the flour directly over a plexiglas plate, without walls.

## 8. Phase Measurements on Polystyrene Foam

To test what was needed to determine optical path lengths, within the GASMAS setup, a simple homodyne modulation system was set up. Polystyrene foam was the scattering medium of choice, because of its high scattering and low absorption nature. Also, the results could be compared with results from time resolved measurements [14].

### 8.1 Setup of a Homodyne Measuring system

The diode laser, SHARP LT031MDO 0-30, was fed with an operating current of 44 mA and its temperature was 48.5 °C. Through the internal bias tee of the diode holder, the diode was modulated by a signal coming from the signal generator. The one used for these experiments was a Rhode&Schwarz SML 01 signal generator. It is capable of producing sine shaped signals at frequencies between 9 kHz and 1.1 GHz. The bias tee is, according to its specification, capable of frequencies well up to 1 GHz. The laser light was brought through an optical fibre and transilluminated the scattering medium. Before the laser light was detected by the Hamamatsu R5070 PMT, it was partially blocked using a mask with an aperture with a diameter of 5.4 mm. Background light was hindered by an optical high pass filter, with a cut off wavelength of 715 nm. The PMT itself was only sensitive up to 900 nm. Thus the light was band pass filtered. The signal from the detector was amplified using a Hamamatsu C6438 wide bandwidth amplifier. The gain of the amplifier is 20 dB up to 50 MHz, where it begins to drop, but the amplification is reasonable even up to 100 MHz. This signal was then sent to an oscilloscope, Tektronix TDS 520B. The signal from the signal generator was also split using a Mini-Circuits ZFRSC-2050 power divider, and sent to the oscilloscope. Both the signal generator and the oscilloscope were connected via GPIB (General Purpose Interface Bus) to a computer. The setup can be seen in Fig. 8.1.

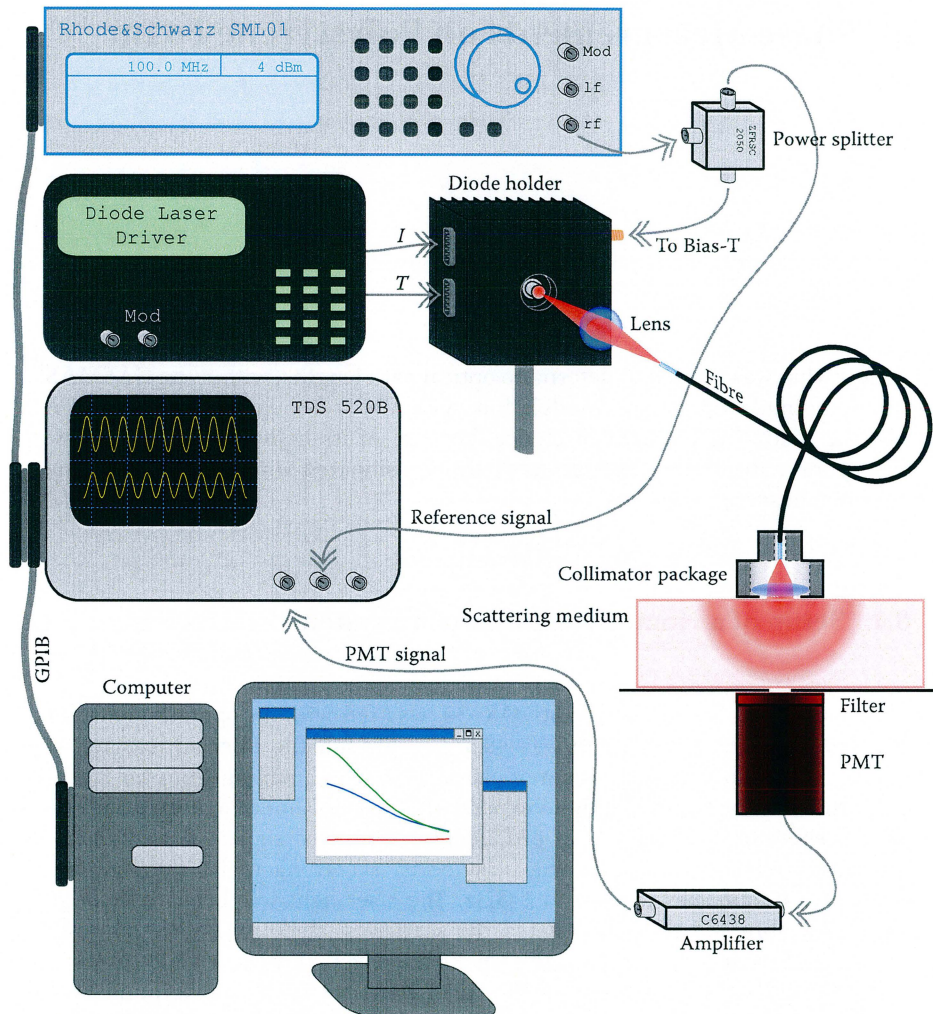


Figure 8.1: Setup of a homodyne modulation system used for phase measurements.

When the equipment initially was tested, there were a lot of noise with frequencies around 110 MHz; possibly interference from FM radio broadcasts. At first, no amplifier was used, but then the signal drowned in noise. To reduce the noise, all of the detector area, including the PMT power supply and amplifier, were provisory screened using aluminium foil. Also cables were changed, when possible to shorter. All inputs and outputs were seen to have  $50 \Omega$  impedance. The noise got smaller, but was still too large compared to the signals coming from the laser light. After a lot of detective work and aluminium foil, an important source of noise was found. It was the cables between the laser driver and the

diode holder, poorly shielded as they were, that functioned as antennas. Efforts were made to screen these, but nothing seemed to work. Possibly, the cables have to be changed to better ones. Although, when the signal from the PMT was amplified and the cables to the diode holder were placed in a noise minimising position, the signal was clear enough for measurements up to about 100 MHz. To reduce the noise even more, a good thing would have been to separate the signal and detection equipment. This was not done though, because of the work involved with fibre coupling.

## **8.2 Method of Phase Measurements**

When the setup was finished and noise was sufficiently reduced, a measurement procedure could be decided.

### **8.2.1 Measurement Procedure**

Three types of measurements were conducted to determine the phase shifts originating from the scattering medium. The first was a noise measurement, where the detector was fully blocked from any light. The noise was therefore only caused by, e.g., FM radio, reflections in the cables and interference between them. The second measurement was to test the phase shifts caused by the system itself, see Eq. 3.12. Instead of transilluminating a scattering medium, an optical filter, reducing the light intensity, was placed above the detector. The aperture was also introduced. In the last measurement, the filter was replaced by the polystyrene foam. Since the phase was found to vary when the voltage over the PMT was changed, this had to be kept constant. This effect has also been described in Ref. [17]. All three types of signals were measured at the same frequencies. A Labview program, earlier developed in the group, was used to record the signals from the oscilloscope. The program was also modified so that it could control the signal generator and automatic frequency sweeps could be run.

### **8.2.2 Data Evaluation**

A further Labview program was developed to fit the data from the oscilloscope with sine functions. From these fittings the DC, AC, and phase components could be retrieved. The phase of the signal was defined as the difference between the reference and the PMT signal phase components. The phase shift caused by the scattering medium could be calculated by subtracting the phase of the foam measurement from the phase of the filter measurement. To calculate the absorption and scattering coefficients of the material, the phase of the scattering medium as a function the frequency, was fitted to the argument of the Green's function in the frequency domain for a transilluminated infinite slab; Eq. A2.3.

The fitting was made with a version of MATLAB's `NLINFIT` routine, improved by Tomas Svensson. The `NLINFIT` is a nonlinear least-square data fitting, using the Gauss-Newton method.

### 8.3 Preliminary Measurements

The preliminary measurements were made to test the setup and the automated device controlling. Data were collected at 27 frequencies, from 50 MHz to 180 MHz in steps of 5 MHz. Before the signals were sent to the computer, five sweeps were averaged on the oscilloscope. The voltage over the PMT was set to 592 V. Measurements were made on a slab of polystyrene foam with a thickness of 29.5 mm. It was about 15 cm x 15 cm in the other directions.

#### 8.3.1 Basic Results

The reference signals DC components were about -0.01 V at all frequencies and for all types of measurements. Their AC components had a distinct frequency dependence; see Fig. 8.2. In all of the following figures, the red represents the noise measurements, the blue the measurements with the filter, and the green the measurements on polystyrene foam. The different behaviour of the reference signal, when measuring noise, is because the laser was turned off.

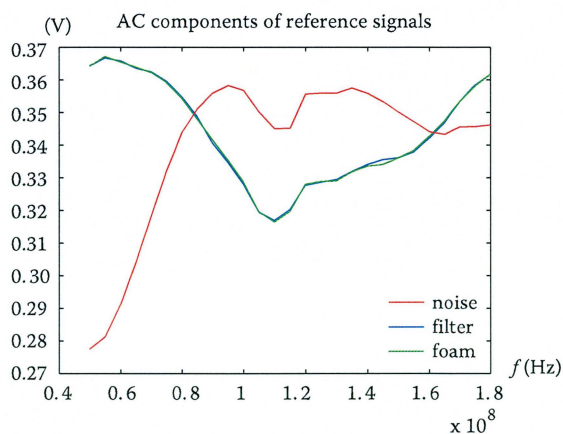


Figure 8.2: Variations in the AC components of the reference signals, as a function of frequency.



The PMT signals DC components can be seen in Fig. 8.3. The noise signal is constant and just below the zero level. The two other signals get irregular at about 100 MHz.

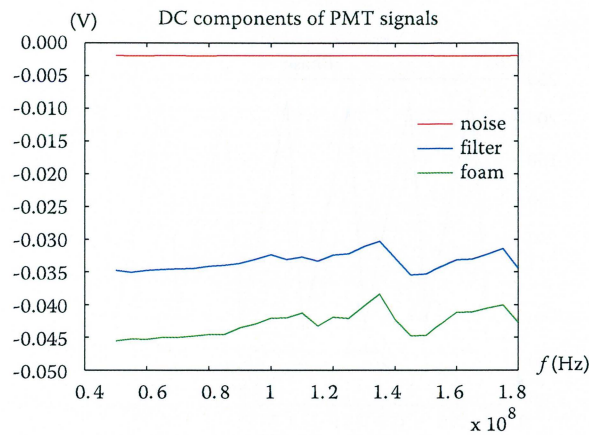


Figure 8.3: The DC components of the PMT signals, as a function of frequency.

The AC component of the foam signal decreased with increasing frequency as expected, but also the signal from the filter measurements decreased in amplitude. This was mainly because of the decreasing gain from the amplifier but also an effect of the limitations of the oscilloscope. As can be seen above 100 MHz, the filter and the foam signals got quite small compared to the noise.

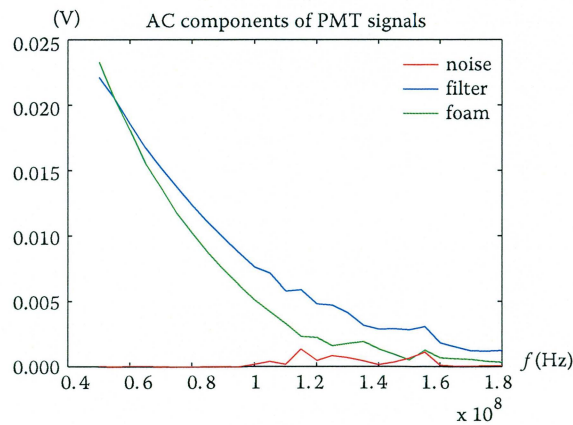


Figure 8.4: The AC components of the PMT signals, as a function of frequency.

The measured phase between the PMT signal and the reference signal can be seen in Fig. 8.5. This shows that the phase changes more because of the system itself than of the scattering medium. The phase decreases about  $18^\circ - 19^\circ$  per MHz as an effect of the components in the setup.

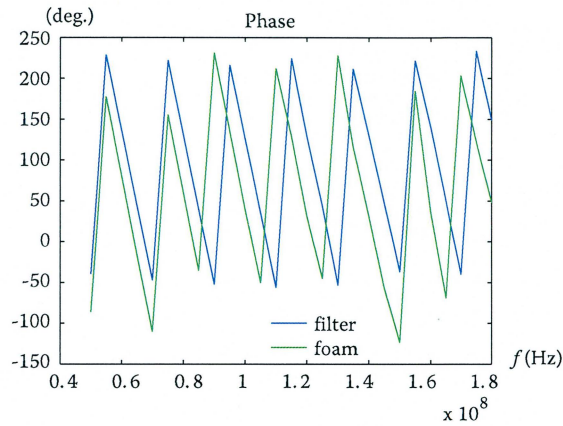


Figure 8.5: The phase shifts of the filter and the foam signals as a function of frequency.

This results in a phase shift, due to the scattering medium, as shown in Fig. 8.6. It is clear that the noise has made the signals too distorted to extract reasonable phase information somewhere above 100 MHz.

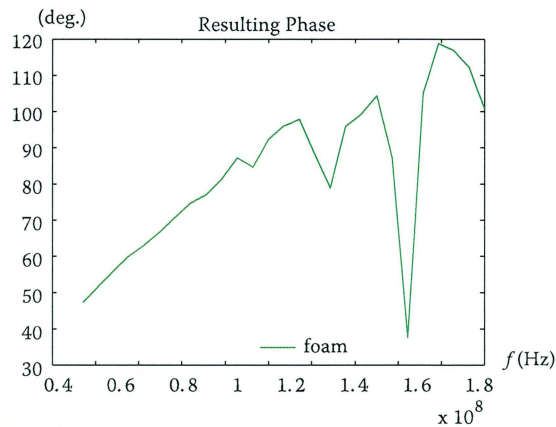


Figure 8.6: The phase shifts due to the polystyrene foam as a function of frequency.

### 8.3.2 Evaluation

An attempt to fit the phase shifts for all of the frequencies, as in Fig. 8.6, led to unrealistic results as one could imagine. This set of phases led to the result that  $\mu_a$  was  $-2.5 \text{ m}^{-1}$  and  $\mu_s$  was  $1400 \text{ m}^{-1}$ . When only taking the first eleven phases into account, a more reasonable conclusion was made. The coefficients were now found to be  $0.05 \text{ m}^{-1}$  and  $2600 \text{ m}^{-1}$ , respectively. The fit and error can be seen in Fig. 8.7. When the data were fitted, the speed of light was assumed to be the speed of light in vacuum. Also, only the first five terms of the Green's function were being used.

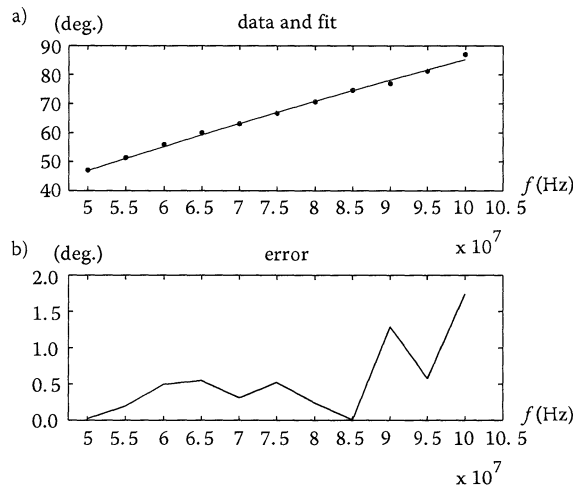


Figure 8.7: a) Measured phase shifts due to the polystyrene foam and a fit to the argument of the Green's function for a transilluminated infinite slab. b) The absolute difference between the phase shifts and the fit.

## 8.4 Extensive Measurements

More extensive measurements were made on the same piece of polystyrene foam, but on a different part of the slab. Data were now collected at 50 frequencies, from 10 MHz to 108 MHz in steps of 2 MHz. Five averages were made on the oscilloscope. The voltage over the PMT was set to 540 V.



### 8.4.1 Basic Results

Since the frequencies were lower during the second measurement, the noise level was lower as well. The frequency dependence of the modulation of the reference signals is illustrated in Fig 8.8. This time the laser was on during the noise measurements, which made all measurements of the reference follow the same curve.

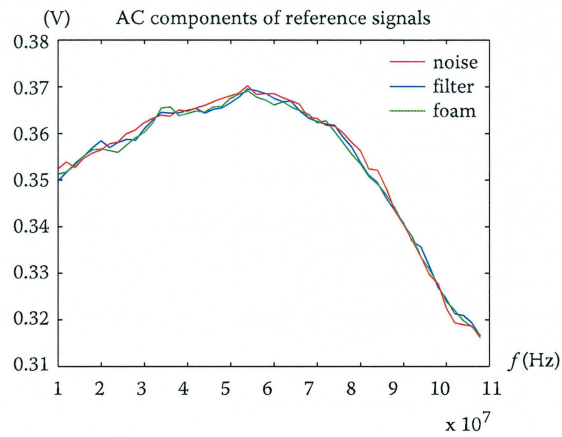


Figure 8.8: The modulation of the reference signals as a function of frequency.

The AC components of the PMT signals were during the whole measurement much larger than the noise. They are presented in Fig 8.9.

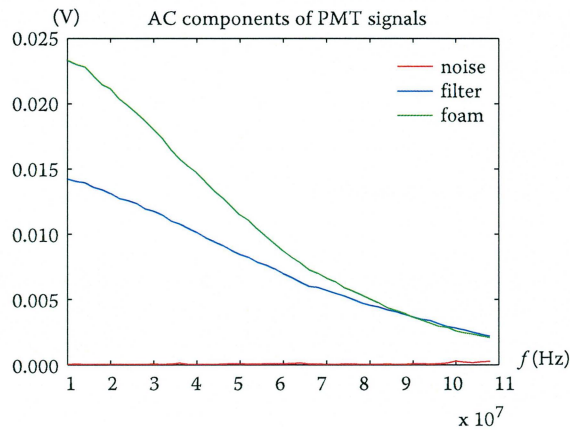


Figure 8.9: The AC components of the PMT signals as a function of frequency.

The phase difference between the PMT signal and the reference signal was still about  $18^\circ - 19^\circ$  per MHz for the measurement with the filter. The phase difference for both the filter and the foam is shown in Fig. 8.10.

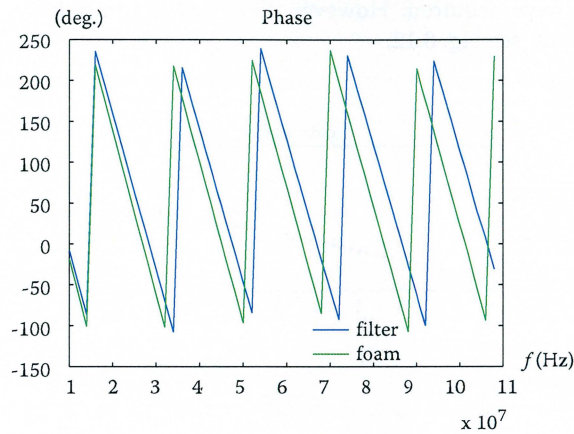


Figure 8.10: The phase shift of the filter and the foam signals as a function of frequency.

The phase shift due to the polystyrene foam showed, this time, a much more regular behaviour, see Fig. 8.11.

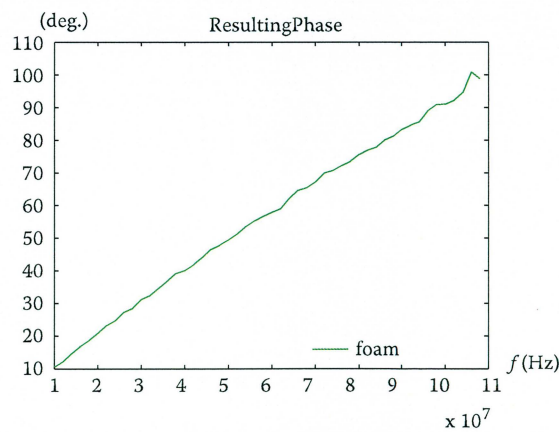


Figure 8.11: The sample imposed phase shift as a function of frequency.

### 8.4.2 Evaluation

Again, the first five terms of the Green's function were used in the calculation of the absorption and scattering coefficient. The same speed of light was also used. When using the whole set of phases, the coefficients  $\mu_a = 0.51 \text{ m}^{-1}$  and  $\mu_s = 3300 \text{ m}^{-1}$  were acquired. However, this resulted in a large error for the second last point, see Fig. 8.12.

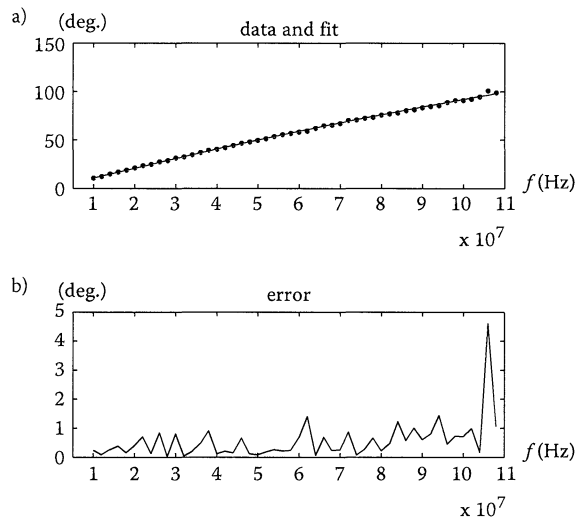


Figure 8.12: a) The shifts in phase due to the polystyrene foam fitted with the argument of the Green's function for a transilluminated slab. b) The absolute difference between the phase shifts and the fit.

When the two last frequencies were removed, the coefficients changed to  $\mu_a = 0.31 \text{ m}^{-1}$  and  $\mu_s = 3100 \text{ m}^{-1}$ . The errors were with this fit smaller; see Fig. 8.13.

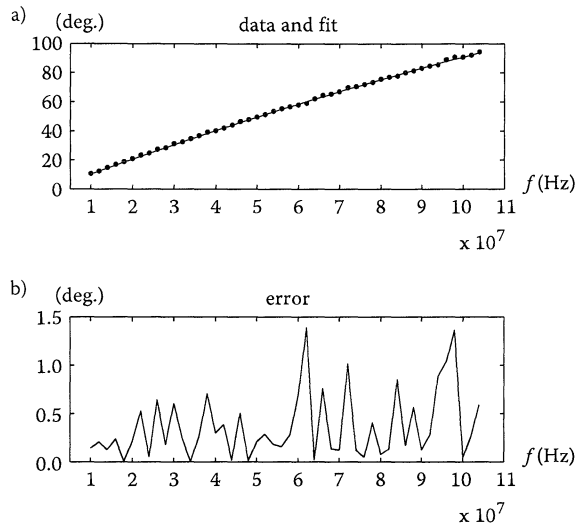


Figure 8.13: a) The first 48 phase shifts due to the polystyrene foam fitted with the argument of the Green's function for a transilluminated slab. b) The absolute difference between the phase shifts and the fit.

## 8.5 Optical Properties of Polystyrene Foam

When comparing the phase series from the two measurements, one sees that they do not fully agree with each other, see Fig. 8.14. What makes this difference is unclear; it could be because of a dent in the piece of foam, since the two series were not measured on the same spot. It could also be some other variation between the measurements. The more extensive series was more carefully conducted, with some additional screening and a higher overall precision. It is thus likely that the second series is the more relevant. According to prior time resolved measurements on polystyrene foam, its absorption and scattering coefficients are  $\mu_a = 0.2 \text{ m}^{-1}$  and  $\mu_s = 4000 \text{ m}^{-1}$  [14]. This is also quite close to the values extracted here,  $\mu_a = 0.31 \text{ m}^{-1}$  and  $\mu_s = 3100 \text{ m}^{-1}$ . These values result in a mean time of 2.9 ns or an equivalent path length of 87 cm, under the condition that the speed of light is the same as in vacuum. With a foam porosity of 98 % [14], that is almost the case. With the time resolved measurement values from Ref. [14], the equivalent mean path length was calculated to 1.1 m.

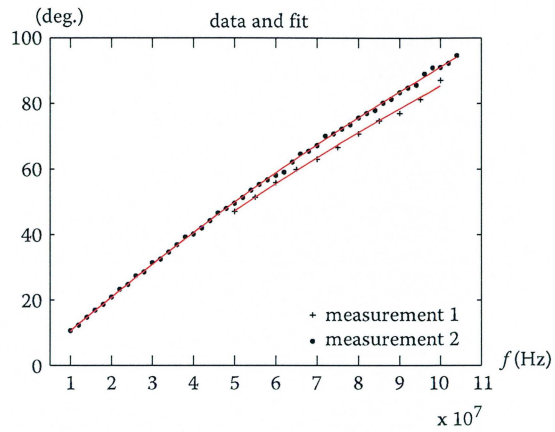


Figure 8.14: The phase shifts from both series of measurements along with their fits.

To see whether the size of the aperture affected the measurements, a calculation of the equivalent mean path length as a function of the distance was made. This can be seen in Fig. 8.15. The path lengths get longer with increasing lateral injection-detection separation. However, in this case, the change is only a couple of centimetres and should not affect the measurements much.

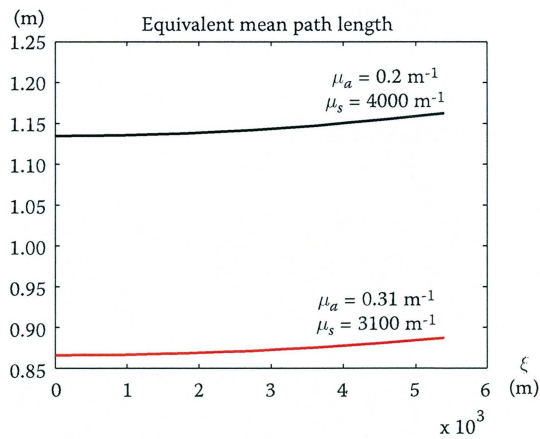


Figure 8.15: Theoretical equivalent mean path lengths for two different sets of absorption and scattering coefficients as a function of lateral injection detection separation.

If the phase shift could have been measured at higher frequencies, the accuracy of the calculated path length could have gotten higher. In Fig. 8.16, the phase shifts, for the absorption and scattering coefficient determined here and for the coefficients from the time resolved measurements, are shown as a function of frequency. One sees clearly that the two curves get more separated as the frequency gets higher.

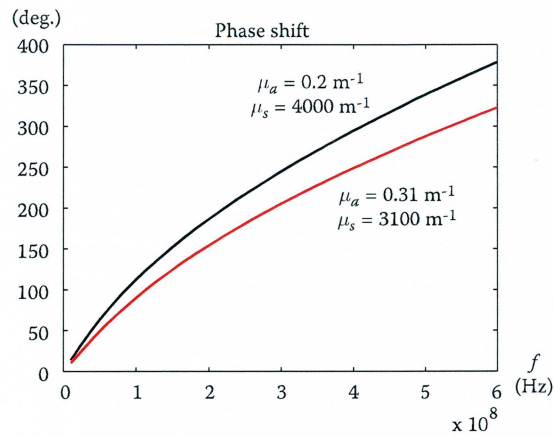


Figure 8.16: Theoretical phase shifts for two different sets of absorption and scattering coefficients as a function of modulation frequency.

## 9. Summary and Conclusions

Within this work, several laser diodes have been tested. A GASMAS setup has been set up and tested, as well as a homodyne phase measuring system. GASMAS measurements were conducted on wheat flour and the optical path length in a slab of polystyrene foam was determined with the phase measuring system.

### 9.1 Experimental Results

#### 9.1.1 Laser Diodes

One of the laser diodes, SHARP LT031MDO 0-30, was found suitable for GASMAS measurements on molecular oxygen. It could reach three consecutive lines in the oxygen A-band; R5R5, R3Q4, and R3R3. This diode was used in all of the experiments that followed in this work.

#### 9.1.2 GASMAS Setup

A new GASMAS arrangement, for molecular oxygen measurements, was successfully put together and tested. Efforts were made to measure the change in GASMAS signal with changing wheat flour density. However, too severe difficulties were discovered and the experiment had to be aborted.

#### 9.1.3 Phase Measurements on Polystyrene Foam

Two sets of phase measurements were done on a 29.5 mm slab of polystyrene foam. The second one was the most extensive and precise measurement. The phase shift caused by the scattering material was measured at frequencies between 10 MHz and 108 MHz. The polystyrene was found to have a scattering coefficient of  $3100 \text{ m}^{-1}$  and an absorption coefficient of  $0.31 \text{ m}^{-1}$ . This corresponded to an optical path length of 87 cm. This value was a bit lower than

the 1.1 m which was determined from a time resolved measurement in Ref. [14]. This difference may depend on the uncertainty of the measurements or some throughout structural error. What could improve the method is to run more tests of what phases are introduced by the system itself. The different results in the two sets of measurements may indicate that the PMT induces a constant phase error, since the PMT voltage was different between the two sets. The measurements would also be improved by using larger frequencies. However, the results are reasonably close for a first version of the setup.

## 9.2 Future Work

This work constitutes the start of a construction project of a GASMAS system where the optical path length can be measured without having to move the sample to another setup. Thus, the path length and the GASMAS signals can be measured at exactly the same position of the sample, which would increase the reliability of the results. However, improvements of the technique are needed. System-induced phase errors, such as of those due to the PMT, have to be investigated. If the amplifier is changed to a faster one, measurements could be done at higher frequencies, which would increase the reliability. With higher frequencies, the problem of recording the signal on the oscilloscope comes, though. Therefore, it would be better if the high frequency is down converted with heterodyning or SSB techniques. If that is done into the kHz regime, the phase difference between the reference and the PMT signal could automatically be detected with, e.g., the lock-in amplifier which possesses such features.



## Acknowledgements

First of all I would like to thank my supervisor, *Prof. Sune Svanberg*, for letting me take part in this fascinating field of research, and for all his help and valuable ideas.

*Linda Persson* has been helpful in every way. The setup of the GASMAS system would have been much too difficult without her help.

I would also like to thank *Mikael Sjöholm* for his help with the LabView programming, and the constructive critique of the manuscript of this thesis. Furthermore, he has been really supportive in the lab.

*Tomas Svensson* solved the problem with the fitting of the scattering and absorption coefficients. He has also made the light transport clearer.

The experimental knowledge of *Janis Alnis* has been highly appreciated.

Thank you all in the Atomic Physics Department, especially *Gabriel Somesfalean*, *Rasmus Grönlund*, *Magnus Bengtsson*, *Gao Hong*, and *Billy Kaldvee*.

Finally, I would like to thank my family and friends, for all backing support. A special thanks to *Matilda Padoan* for making my life so joyful.

This work was financially supported by the Swedish Research Council (VR) and by AstraZeneca.

## References

- [1] G. P. Agrawal, N. K. Dutta, *Semiconductor Lasers*, 2nd ed. (Van Nostrand Reinhold, New York 1993)
- [2] O. Svelto, *Principles of Lasers*, 4<sup>th</sup> ed. (Plenum Press, New York 1998)
- [3] U. Gustafsson, *PhD Thesis, Diode laser spectroscopy in extended wavelength ranges*. (Lund Institute of Technology, Lund 2000)
- [4] B. Chance, M. Cope, E. Gratton, N. Ramanujam and B. Tromberg, *Phase measurement of light absorption and scatter in human tissue*. Rev. Sci. Instr. **69**, 3457-3481 (1998)
- [5] S. R. Arridge, M. Cope, and D. T. Delpy, *The theoretical basis for the determination of optical pathlength in tissue: temporal and frequency analysis*. Phys. Med. Biol. **37**, 1531-1560 (1992)
- [6] J. B. Fishkin, and E. Gratton, *Propagation of photon-density waves in strongly scattering media containing an absorbing semi-infinite plane bounded by a straight edge*, Opt. Soc. Am. A **10**, 127-140 (1992)
- [7] I. V. Yaroslavsky, A. N. Yaroslavsky, V. V. Tuchin, and H.-J. Schwarzmaier, *Effect of the scattering delay on time-dependent photon migration in turbid media*, Appl. Opt. **36**, 6529-6538 (1997)
- [8] C. Eker, *PhD Thesis, Optical characterization of tissue for medical diagnostics*. (Lund Institute of Technology, Lund 1999)
- [9] M. Kohl, R. Watson, and M. Cope, *Optical properties of highly scattering media determined from changes in attenuation, phase and modulation*. Appl. Opt. **36**, 105-115 (1997)
- [10] S. Svanberg, *Atomic and Molecular Spectroscopy — Basic Aspects and Practical Applications*, 3rd ed. (Springer, Berlin, Heidelberg 2001)

- [11] P. Kauranen, *PhD Thesis, Near-infrared diode laser frequency-modulation spectroscopy for high-sensitivity gas analysis*. (Lund Institute of Technology, Lund 1995)
- [12] The HITRAN Database, <http://cfa-www.harvard.edu/HITRAN/>
- [13] M. Sjöholm, G. Somesfalean, J. Alnis, S. Andersson-Engels, and S. Svanberg, *Analysis of gas dispersed in scattering media*, *Opt. Lett.* **26**, 16-18 (2001)
- [14] G. Somesfalean, M. Sjöholm, J. Alnis, C. af Klinteberg, S. Andersson-Engels, and S. Svanberg, *Concentration measurement of gas embedded in scattering media by employing absorption and time-resolved laser spectroscopy*. *Appl. Opt.* **41**, 3538-3544 (2002)
- [15] J. Alnis, B. Anderson, M. Sjöholm, G. Somesfalean, and S. Svanberg, *Laser spectroscopy on free molecular oxygen dispersed in wood materials*. *Appl. Phys. B* **77**, 691-695 (2003)
- [16] S.-G. Pettersson, S. Borgström, and H. Hertz, *Optisk Teknik, Advanced Optics*, (Lund Institute of Technology, Lund 1999)
- [17] N. Ramanujam, C. Du, H. Y. Ma, and B. Chance, *Sources of phase noise in homodyne and heterodyne phase modulation devices used for tissue oximetry studies*. *Rev. Sci. Instr.* **68**, 3042-3054 (1998)

## Appendix A

### Analytic expressions of the behaviour of light in scattering media

This Appendix gives analytic expressions for the Green's function in the time and frequency domain, the phase shifts, and the mean time of flight. Expressions are given for the following geometries: infinite medium, semi-infinite half-space, and infinite slab for both transillumination and reflection measurement. For other geometries (2D circle, finite and infinite cylinder, and sphere) the reader is referred to the article by Arridge et al. [5]

The expressions are abbreviated by the definitions

$$\begin{aligned}z_0 &= 1/\mu_s \\ \rho &= \sqrt{\xi^2 + z_0^2} \\ z_{+n} &= (2n+1)d + z_0 \\ z_{-n} &= (2n+1)d - z_0 \\ z_{+n'} &= 2nd + z_0 \\ z_{-n'} &= 2nd - z_0 \\ \rho_{+n'} &= \sqrt{\xi^2 + z_{+n'}^2} \\ \rho_{-n'} &= \sqrt{\xi^2 + z_{-n'}^2} \\ \alpha &= \sqrt{\mu_a c + i\omega} / \gamma \\ \sigma &= \sqrt{\mu_a c} / \gamma \\ A &= \left( (\mu_a c)^2 + \omega^2 \right)^{1/4} / \gamma \\ \tau &= \arctan(\omega / \mu_a c)\end{aligned}$$

The  $\xi$  denotes the lateral injection-detection separation and  $\omega$  is the angular frequency of the modulation. The time is  $t$ , and the delay of the scattering is  $t'$ . However, this delay  $t' = z_0/c$ , can in most cases be said to be 0. If that is not the case,  $t'$  has to be added to the mean times and  $-\omega t'$  to  $\psi$ . For the case of the infinite slab it is only necessary to count the first five terms of the infinite sum, to achieve a high precision.

## A1. Green's Functions in the Time Domain

Infinite medium

$$g_{inf}(d, t, t') = \left( d / \left( 2(4\pi\gamma^2)^{3/2} (t-t')^{5/2} \right) \right) \exp \left( - \left( \mu_a c (t-t') + \frac{d^2}{4\gamma^2 (t-t')} \right) \right) \quad (\text{A1.1})$$

Semi-infinite half-space

$$g_{half}(\xi, z_0, t, t') = \left( z_0 / \left( (4\pi\gamma^2)^{3/2} (t-t')^{5/2} \right) \right) \exp \left( - \left( \mu_a c (t-t') + \frac{\rho^2}{4\gamma^2 (t-t')} \right) \right) \quad (\text{A1.2})$$

Infinite slab  $0 < z < d$  (evaluated at  $z = d$ )

$$g_{slab}(\xi, z_0, t, t') = \frac{-\exp \left( - \left( \mu_a c (t-t') + \xi^2 / 4\gamma^2 (t-t') \right) \right)}{(4\pi\gamma^2)^{3/2} (t-t')^{5/2}} \cdot \sum_{n=0}^{\infty} \left( z_{+n} \exp \left( \frac{-z_{+n}^2}{4\gamma^2 (t-t')} \right) - z_{-n} \exp \left( \frac{-z_{-n}^2}{4\gamma^2 (t-t')} \right) \right) \quad (\text{A1.3})$$

Infinite slab (evaluated at  $z = 0$ )

$$g_{slab}(\xi, z_0, t, t') = \frac{\exp \left( - \left( \mu_a c (t-t') + \xi^2 / 4\gamma^2 (t-t') \right) \right)}{(4\pi\gamma^2)^{3/2} (t-t')^{5/2}} \left( z_0 \exp \left( \frac{-z_0^2}{4\gamma^2 (t-t')} \right) + \sum_{n=1}^{\infty} \left( z_{+n} \exp \left( \frac{-z_{+n}^2}{4\gamma^2 (t-t')} \right) - z_{-n} \exp \left( \frac{-z_{-n}^2}{4\gamma^2 (t-t')} \right) \right) \right) \quad (\text{A1.4})$$

## A2. Green's Functions in the Frequency Domain

Infinite medium

$$G_{inf}(d, \omega, t') = e^{-i\omega t'} \frac{(1 + \alpha d) e^{-\alpha d}}{2(2\pi)^{3/2} d^2} \quad (\text{A2.1})$$

Semi-infinite half-space

$$G_{half}(\xi, z_0, \omega, t') = e^{-i\omega t'} \frac{(1 + \alpha \rho) z_0 e^{-\alpha \rho}}{(2\pi)^{3/2} \rho^2} \quad (\text{A2.2})$$

Infinite slab  $0 < z < d$  (evaluated at  $z = d$ )

$$G_{slab}(\xi, z_0, \omega, t') = \frac{e^{-i\omega t'}}{(2\pi)^{3/2}} \sum_{n=0}^{\infty} \left( \frac{z_{+n}}{\rho_{+n}} (1 + \alpha \rho_{+n}) e^{-\alpha \rho_{+n}} - \frac{z_{-n}}{\rho_{-n}} (1 + \alpha \rho_{-n}) e^{-\alpha \rho_{-n}} \right) \quad (\text{A2.3})$$

Infinite slab (evaluated at  $z = 0$ )

$$G_{slab}(\xi, z_0, \omega, t') = \frac{e^{-i\omega t'}}{(2\pi)^{3/2}} \left( \frac{z_0}{\rho^3} (1 + \alpha \rho) e^{-\alpha \rho} + \sum_{n=1}^{\infty} \left( \frac{z_{+n'}}{\rho_{+n'}} (1 + \alpha \rho_{+n'}) e^{-\alpha \rho_{+n'}} - \frac{z_{-n'}}{\rho_{-n'}} (1 + \alpha \rho_{-n'}) e^{-\alpha \rho_{-n'}} \right) \right) \quad (\text{A2.4})$$

### A3. Phase Shifts

Infinite medium

$$\psi_{inf}(d) = \arctan\left(\frac{Ad \sin(\tau/2)}{1 + Ad \cos(\tau/2)}\right) - Ad \sin(\tau/2) \quad (\text{A3.1})$$

Semi-infinite half-space

$$\psi_{half}(\rho) = \arctan\left(\frac{A\rho \sin(\tau/2)}{1 + A\rho \cos(\tau/2)}\right) - A\rho \sin(\tau/2) \quad (\text{A3.2})$$

For the infinite slab there exist no analytic expressions. One must therefore numerically take the argument of the Green's function in the frequency domain to get the phase shift.

#### A4. Mean Times

Infinite medium

$$\langle t \rangle_{inf}(d) = \frac{1}{2} \frac{d^2}{\gamma \left( \gamma + d(\mu_a c)^{1/2} \right)} \quad (\text{A4.1})$$

Semi-infinite half-space

$$\langle t \rangle_{half}(\rho) = \frac{1}{2} \frac{\rho^2}{\gamma \left( \gamma + \rho(\mu_a c)^{1/2} \right)} \quad (\text{A4.2})$$

Infinite slab  $0 < z < d$  (evaluated at  $z = d$ )

$$\langle t \rangle_{slab}(\rho) = \frac{1}{2\gamma^2} \frac{\sum_{n=0}^{\infty} \left( \frac{z_{+n}}{\rho_{+n}} e^{-\sigma\rho_{+n}} - \frac{z_{-n}}{\rho_{-n}} e^{-\sigma\rho_{-n}} \right)}{\sum_{n=0}^{\infty} \left( \frac{z_{+n}}{\rho_{+n}^3} (1 + \sigma\rho_{+n}) e^{-\sigma\rho_{+n}} - \frac{z_{-n}}{\rho_{-n}^3} (1 + \sigma\rho_{-n}) e^{-\sigma\rho_{-n}} \right)} \quad (\text{A4.3})$$

Infinite slab (evaluated at  $z = 0$ )

$$\langle t \rangle_{slab}(\xi, z_0) = \frac{1}{2\gamma^2} \frac{\frac{z_0}{\rho} e^{-\sigma\rho} + \sum_{n=1}^{\infty} \left( \frac{z_{+n'}}{\rho_{-n'}} e^{-\sigma\rho_{-n'}} - \frac{z_{-n'}}{\rho_{-n'}} e^{-\sigma\rho_{-n'}} \right)}{\frac{z_0}{\rho^3} (1 + \sigma\rho) e^{-\sigma\rho} + \sum_{n=1}^{\infty} \left( \frac{z_{+n'}}{\rho_{+n'}^3} (1 + \sigma\rho_{+n'}) e^{-\sigma\rho_{+n'}} - \frac{z_{-n'}}{\rho_{-n'}^3} (1 + \sigma\rho_{-n'}) e^{-\sigma\rho_{-n'}} \right)} \quad (\text{A4.4})$$